Towards Understanding the Non-Fermi-Liquid Behaviour of MnSi

Andrei Berceanu*

Zernike Institute for Advanced Materials, University of Groningen, Nijenborgh 4, 9747 AG Groningen, The Netherlands

(Dated: August 19, 2008)

MnSi is one of the most extensively studied ferromagnets. The Curie temperature of MnSi is 29.5 K at ambient pressure, but vanishes above a critical pressure of 14.6 kbar. MnSi shows a first order quantum phase transition from a ferromagnetic to a paramagnetic phase. In its normal state, MnSi displays an enigmatic $T^{3/2}$ low-temperature dependence of the resistivity, defying the T^2 law that follows from Landau's Fermi liquid theory, the "standard model for metals". After reviewing Landau's Fermi liquid theory, this paper emphasizes the possible routes that might lead to its breakdown. The goal is to understand the non-Fermi-liquid phase of MnSi. High-precision measurements of its electrical transport and magnetic properties, as well as neutron scattering experiments are discussed. Finally, various evidence of spontaneous skyrmion ground states in MnSi is presented. The presence of such states could explain the peculiar $T^{3/2}$ power law dependence.

Contents

Preamble

Loosely speaking, one defines a phase transition as a transformation of a thermodynamic system from one state to another. Phase transitions are among the most fascinating phenomena in nature. They also have far-reaching implications. The liquid-gas and solid-liquid transitions in water, for instance, are common occurrences of obvious importance. As anybody who has ever melted ice for drinking water is painfully aware, both transitions are first order, or discontinuous, at ambient pressure (Fig. 1(a)): the density changes discontinuosly across the transition, and a latent heat is present – the temperature does not change, despite continued energy input, until all of the ice has melted.

The transition from a paramagnetic phase to a ferromagnetic one in the elements iron, nickel, and cobalt made possible the invention of the compass! These examples (and many others) demonstrate that phase transitions come in a wide variety of phenomenologies with no entirely obvious unifying features. Accordingly, early attempts at a theoretical understanding of phase transitions focused on particular examples. Notably, the famous dutch scientist van der Waals (1873) described the liquid-gas transition by developing the first example of what was later to become known as a *mean-field theory*. Weiss (1907) gave a mean-field theory of ferromagnetism that was based on the concept of the mean field seen by each "elementary magnet" (spin had yet to be discovered at that time) that is produced by all other elementary magnets.

Finally, a unification of all mean-field theories was achieved by Landau (1965). He introduced the general concept of the *order parameter*, a thermodynamic observable that vanishes in one of the two phases and is nonzero in the other. The former is called the *disordered phase* – in the sense of "phase without long-range order" – and the latter the *ordered phase*. In the case of the ferromagnet, the order parameter is the magnetization; in the case of the liquid-gas transition, the order parameter is the density difference between the two phases.

The theoretical understanding of classical, or thermal, phase transitions, which occur at a nonzero temperature, is very well developed. *Quantum phase transitions*, which occur at zero temperature as a function of some nonthermal control parameter such as composition or pressure, are not yet as well understood.

The structure of this paper is as follows. Section I gives a brief introduction to the modern theory of phase

*Electronic address: A.C.Berceanu@student.rug.nl

transitions, both classical and quantum. In Section II I present some concepts behind Landau's Fermi liquid, the "standard model" for metals, and also various routes that might lead to its breakdown. In Section III I will apply these concepts to the case of MnSi, which shows a Fermi-liquid to non-Fermi-Fermi liquid transition. Both experimental and theoretical results will be reviewed. Finally, Section IV concludes with a summary and a discussion of open problems.

I. PHASE TRANSITIONS

The ferromagnet-paramagnet transition is less frequently observed, as the most common ferromagnets, such as iron and its alloys, lose their ferromagnetic properties only at a temperature T_c (usually called Curie temperature) far above room temperature. Nevertheless, it is well known that this transition, in the absence of a magnetic field, is second order, or continuous: the magnetization rises continuously from zero as the temperature is lowered below T_c, as shown in Fig. 1.

Theorists have for some time studied the properties of a *quantum ferromagnetic phase transition* that is characterized by keeping the temperature at absolute zero, $T = 0$ K, and varying some control parameter. The fluctuations that drive quantum phase transitions are of a different nature from those at $T > 0$, so one expects a different behaviour.

According to the third law of thermodynamics, $T = 0$ cannot be reached experimentally. But the properties of matter at a few kelvin, are often dominated by what would go on at 0 K. Quantum phase transitions are governed by the laws of quantum statistical mechanics, according to which a system at $T = 0$ resembles, in some aspects, the corresponding system at $T > 0$ in more than three spatial dimensions. Thus quantum phase transitions are possibly easier to describe theoretically than those at $T > 0$, because Landau's mean-field theory of phase transitions becomes exact in sufficiently high dimensions, as we will see in Sec. I.A. This property led Hertz (1976) to predict that the quantum ferromagnetic transition in metals should be second order, and described by Landau theory.

MnSi becomes magnetic below 29.5 K and T_c can be further supressed by applying hydrostatic pressure; Fig. 2 shows a schematic phase diagram.[1] The pressure tuning of T_c provides a way to study the transition at very low temperatures.

Actually, Uemura *et al.* (2007) have used a muon spin relaxation technique to *show convincingly* that the transition in MnSi is *first order*.

So what went wrong in Hertz theory? Landau theory can describe both first-order and second-order transitions, depending on the presence and the signs of various terms in the mean-field free energy. The presence or absence of terms is governed by basic symmetry properties and must be the same for all systems that belong to a particular class, for instance Heisenberg ferromagnets. The signs, by contrast, depend on the band structure of a given material, and thus may differ from material to material. But it is extremely unlikely that these microscopic details conspire to render the quantum ferromagnetic transition first order. It is more likely that there is a universal explanation for the observations – namely, the notion that a correct description of any phase tran-

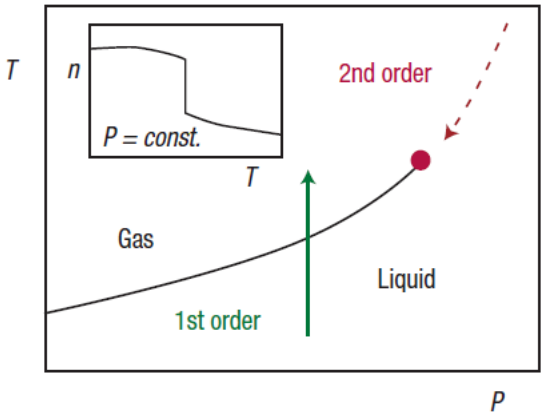

(a)The temperature-pressure (T-P) phase diagram for a fluid.

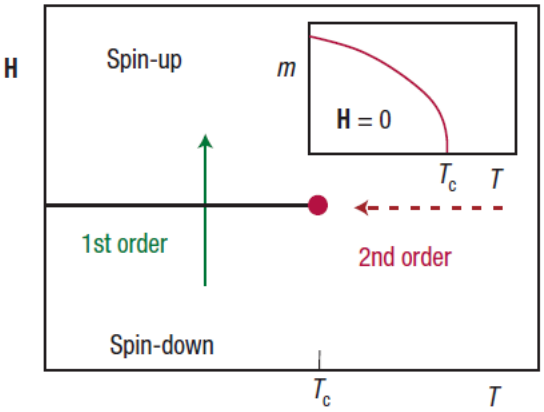

(b)The magnetic field-temperature ($\boldsymbol{H}$-T) phase diagram for a ferromagnet.

FIG. 1 These two phase diagrams are topologically identical. The phase separation line (solid black line) ends at a critical point (red circle). The green solid arrows show paths corresponding to first-order transitions. This path is the default for heating a liquid at constant pressure. The red dashed arrows show paths corresponding to second-order transitions. This path is the default for a magnet in a vanishing magnetic field. The insets qualitatively show the density n as a function of the temperature at constant pressure for the first-order liquid-gas transition and the magnetization m as a function of the temperature in zero magnetic field for the second-order ferromagnetic transition, respectively. Figure from Belitz and Kirkpatrick (2007).

[1] Strictly speaking, MnSi is a helimagnet, not a ferromagnet.

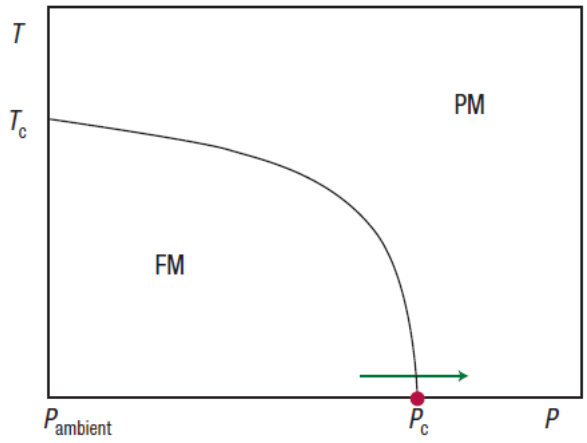

FIG. 2 Magnetic T-P phase diagram for materials such as UGe_2, $ZrZn_2$ or MnSi. The solid black curve separates a ferromagnetic (FM) phase from a paramagnetic (PM) one. The red dot denotes the quantum phase transition, and the green arrow represents an experimentally accessible path. Figure from Belitz and Kirkpatrick (2007).

sition must take into account low-energy excitations, or *soft modes*, that couple to the order parameter.

This principle is well known in the context of classical phase transitions and it applies to quantum phase transitions as well (Belitz *et al.*, 2005). In metals at $T = 0$, particle-hole excitations about the Fermi surface constitute such soft modes, and in Hertz theory they are treated too crudely for a reliable description of the transition. Treating these excitations more carefully leads to the conclusion that quantum ferromagnetic transitions in metals are generally discontinuous.

Since Landau theory underlies all later theories of phase transitions, I will briefly present its general features and main results in Sec. I.A.

A. Landau Theory of Phase Transitions

Landau theory is based on one crucial assumption, namely, that the free energy F is an analytic function of the order parameter m, and hence can be expanded in a power series:

$$F \approx F_L(m) = rm^2 + vm^3 + um^4 + \mathcal{O}(m^5) \qquad (1.1)$$

Here r, v, u, etc., are parameters of the Landau theory that depend on all degrees of freedom other than m. The *physical* value of m is the one that *minimizes* F_L.

Landau theory is remarkably versatile. For sufficiently large r, the minimum of the free energy is always located at $m = 0$ (the system is in the disordered phase), while for sufficiently small r, the minimum is at some $m \neq 0$ (ordered phase). If $v \neq 0$, the transition from $m = 0$ to $m \neq 0$ occurs discontinuously, i.e., it is of *first order*. An example of such a transition is the liquid-gas one. If, either accidentally or for symmetry reasons, $v = 0$, then the theory describes a *second order (continuous) transition*, or *critical point*, at $r = 0$. A good example is the ferromagnetic transition in zero applied magnetic field. Thus r is measuring the distance from the critical point, $r \propto (T - T_c)$ for a thermal transition.

Furthermore, Landau theory applies to both classical and quantum systems, including systems at zero temperature. In the latter case, the free energy $F = U - TS$ reduces to the internal energy U, since $T = 0$. For the finite temperature case, a stable phase could have a higher internal energy U than an unstable one, as long as its entropy S was also higher. At $T = 0$, however, the stable phase must represent a minimum of the internal energy.

Within Landau theory, the qualitative behaviour of all critical points is identical. Specifically, the order parameter vanishes as $m = \sqrt{-r/(2u)}$ when the critical point is approached from the ordered phase. This is an example of the so-called super-universality of Landau theory. The critical exponent β which describes the singularity of the order parameter at the critical point via $m \propto |r|^\beta$, is predicted to have the mean-field value of $\frac{1}{2}$ for all critical points. Universality of the critical exponents is actually observed in experiments but it is weaker than the super-universality predicted by Landau theory, and the exponential values are in general different from what Landau theory predicts. Moreover, the exponent values turn out to be dimensionality dependent. For instance, all three-dimensional Ising magnets have $\beta = \frac{1}{8}$. Three-dimensional ferromagnets with $O(3)$ Heisenberg symmetry also have a common value of $\beta \approx 0.35$ but it is different from that in Ising magnets.

The reason for the failure of Landau theory to correctly describe the critical behaviour is that is does not adequately include the fluctuations of the order parameter about its average value. The effects of these fluctuations in general decrease with increasing dimensionality and with increasing number of order parameter components. This explains why the critical behaviour of Ising magnets (one order parameter component) deviates more strongly from Landau theory than that of Heisenberg magnets (three spin components), and why the three-dimensional exponents are closer to the mean-field values than those of two-dimensional systems.

This suggests that Landau theory might actually be correct for systems with sufficiently high dimensionality d. In fact, the fluctuations lead to two different critical dimensionalities, d_c^+ and d_c^- for a given phase transition. If the dimensionality d is larger than the upper critical dimension d_c^+, fluctuations are unimportant for the leading critical behaviour, and Landau theory gives the correct answers. If d is between the upper and the lower critical dimensions, $d_c^+ > d > d_c^-$, a phase transition still exists, but the critical behaviour is different from mean-field theory. For dimensionalities below the critical dimension, fluctuations become so strong that they completely destroy the ordered phase. For the ferromagnetic transition at non-zero temperature, $d_c^+ = 4$, and $d_c^- = 2$ or 1 for Heisenberg and Ising symmetries, respectively.

B. Scaling and the Renormalization Group

As indicated in Sec. I.A, below the upper critical dimension d_c^+, order parameter fluctuations play a crucial role in determining the critical behaviour. To include them, one has to generalize the Landau free energy (1.1) by writing the partition function Z as a functional integral (Wilson and Kogut, 1974)

$$Z = \exp\left(-\frac{F}{T}\right) = \int D[\phi] \exp\left(-S[\phi]\right) \tag{1.2}$$

with the action or Landau-Ginzburg-Wilson (LGW) functional S given by the d-dimensional integral

$$S[\phi] = \frac{1}{T}\int d^d x \left[c\left(\boldsymbol{\nabla}\phi(\boldsymbol{x})\right)^2 + F_L(\phi(\boldsymbol{x})) - h\phi(\boldsymbol{x})\right] \tag{1.3}$$

ϕ is a fluctuating scalar field whose average value is equal to the order parameter $m = \langle\phi\rangle$, and c a constant. (Here, $\langle\ldots\rangle$ denotes the average with respect to the statistical weight $\exp\left(-S[\phi]\right)$). The presence of an external magnetic field h, conjugate to the order parameter, is also included in Eq. (1.3) and the units are such that Boltzmann's constant, Planck's constant, and the Bohr magneton are equal to unity.

In the disordered phase, away from the critical point, the correlation function of the order parameter fluctuations, $G(\boldsymbol{x}-\boldsymbol{y}) = \langle\phi(\boldsymbol{x})\phi(\boldsymbol{y})\rangle$ is short-ranged. When the critical point is approached, the correlations become long-ranged. Their typical length scale, the correlation length ξ, diverges when the distance r from the critical point vanishes

$$\xi \propto |r|^{-\nu} \tag{1.4}$$

Here, ν is the correlation length critical exponent. Close to the critical point, the correlation length ξ is the only relevant length scale in the system. Therefore, the physical properties must be unchanged, if we rescale all lengths in the system by a common factor b, and at the same time adjust the external parameters in such a way that the correlation length retains its old value. This gives rise to the homogeneity relation for the free energy density $f = -\frac{T}{V}\ln Z$ (where V is the total volume of the system)

$$f(r,h) = b^{-d} f(rb^{1/\nu}, hb^{y_h}) \tag{1.5}$$

The scale factor b is an arbitrary positive number, and y_h is another critical exponent. Analogous homogeneity relations for other thermodynamic quantities can be obtained by differentiating f. These homogeneity laws were first obtained phenomenologically by Widom (1965) and are sometimes summarily called the scaling hypothesis. Within the framework of the modern renormalization group theory of phase transitions (Wilson and Kogut, 1974), the scaling laws can be derived from first principles.

In addition to the critical exponents ν and y_h defined above, a number of other exponents are in common use. They describe the dependence of the order parameter and its correlations on the distance from the critical point and on the field conjugate to the order parameter. However, not all of these exponents are independent of each other. Some are inter-connected by so-called scaling relations.

In addition to the diverging length scale ξ, a critical point is characterized by a diverging time scale, the correlation time ξ_t. It leads to the phenomenon of *critical slowing down*, i.e., very slow relaxation towards equilibrium near a critical point. At generic critical points, the divergence of the correlation time follows a power law $\xi_t \propto \xi^z$, where z is the *dynamical critical exponent*.

As mentioned above, the critical exponents display the remarkable phenomenon of universality, i.e., they are the same for entire classes of phase transitions which may occur in very different physical systems. These classes, the so-called universality classes, are determined only by the symmetries of the Hamiltonian and the spatial dimensionality of the system. The physical mechanism behind universality is the divergence of the correlation length. Close to the critical point the system effectively averages over large volumes rendering the microscopic details of the Hamiltonian unimportant.

C. Classical Versus Quantum Phase Transitions

In classical statistical mechanics, statics and dynamics decouple. This can be seen by considering a classical Hamiltonian $H\left(p_i, q_i\right) = H_{\rm kin}\left(p_i\right) + H_{\rm pot}\left(q_i\right)$ consisting of a kinetic part $H_{\rm kin}$ that only depends on the momenta p_i and a potential part $H_{\rm pot}$ that only depends on the coordinates q_i. The classical partition function of such a system

$$Z = \int\prod dp_i e^{-\frac{H_{\rm kin}}{T}} \int\prod dq_i e^{-\frac{H_{\rm pot}}{T}} = Z_{\rm kin} Z_{\rm pot} \tag{1.6}$$

factorizes in kinetic and potential parts which are completely independent of each other. The kinetic contribution to the free energy density will usually not display any singularities, since it derives from a product of simple Gaussian integrals. Therefore, one can study the *thermodynamic* critical behaviour in classical systems using time-independent theories such as the Landau-Ginzburg-Wilson theory discussed in Sec. I.B. As a result of this decoupling, the dynamical critical exponent is completely independent of the thermodynamic ones.

In quantum statistical mechanics, the situation is different. The Hamiltonian H and its parts $H_{\rm kin}$ and $H_{\rm pot}$ are now operators, and $H_{\rm kin}$ and $H_{\rm pot}$ in general *do not commute*. Consequently, the partition function $Z = {\rm Tr}\, e^{-H/T}$ does not factorize, and one must solve for the dynamics together with the thermodynamics. Quantum-mechanical analogues of the Landau-Ginzburg-Wilson theory described by Eq. (1.3) therefore need to be formulated in terms of space and time-dependent fields; they can be derived, e.g., via a functional integral representation of the partition function. The simplest example

of such a quantum Landau-Ginzburg-Wilson functional takes the form

$$S[\phi] = \int_0^{1/T} d\tau \int d^d x \left[a \left(\partial_\tau \phi(\boldsymbol{x}, \tau) \right)^2 + c \left(\boldsymbol{\nabla} \phi(\boldsymbol{x}, \tau) \right)^2 + F_L \left(\phi(\boldsymbol{x}, \tau) \right) - h \phi(\boldsymbol{x}, \tau) \right] \tag{1.7}$$

with τ being the *imaginary time*, and a and c constants. This functional also illustrates another remarkable feature of quantum statistical mechanics. The imaginary time variable τ effectively acts as an additional coordinate. For non-zero temperatures, $1/T < \infty$, the extra dimension extends only over a finite interval. If one is sufficiently close to the critical point so that the condition $\xi_t > 1/T$ is fulfilled, the extra dimension will not affect the critical behaviour. One can thus conclude that the asymptotic behaviour at any transition with a non-zero critical temperature is purely classical. However, a quantum phase transition at $T = 0$ is described by a theory that effectively is in different (higher) dimension. Therefore, it will be in a different universality class!

Using the equivalence between imaginary time and an additional dimension, the homogeneity law for the free energy can be easily generalized to the quantum case (Sachdev, 1999)). For conventional power law dynamical scaling it takes the form

$$f(r, h, T) = b^{-(d+z)} f\left(r b^{1/\nu}, h b^{y_h}, T b^z \right) \tag{1.8}$$

This relation implies that the scaling behaviour of a zero-temperature quantum phase transition in d dimensions can be mapped onto that of some classical transition in $d + z$ spatial dimensions. If space and time enter the theory symmetrically the dynamical exponent is $z = 1$, but in general, it can take any positive value. This quantum to classical mapping is valid for the thermodynamics only! Other properties like the real time dynamics at finite temperatures require more careful considerations (Sachdev, 1999). Moreover, some quantum phase transitions, such as the metal-insulator transition, do no have a classical counterpart and thus the quantum to classical mapping does not dirrectly apply.

It is worth emphasizing that the entire concept of a Landau-Ginzburg-Wilson theory in terms of the order parameter field relies on the order parameter fluctuations being the only soft or gapless mode in the system. If there are other soft modes, e.g., due to conservation laws or broken continuous symmetries, they lead to long-range power-law correlations of various quantities even *away from the critical point*. This phenomenon is called generic scale invariance (Dorfman *et al.*, 1994; Law and Nieuwoudt, 1989; Nagel, 1992). If one insists on deriving a Landau-Ginzburg-Wilson theory for a phase transition in the presence of generic scale invariance, the additional soft modes lead to coefficients that are singular functions of space and time, severely limiting the usefulness of the theory (Belitz *et al.*, 1997; Vojta *et al.*, 1996). In such a situation, one should instead work with a coupled theory that keeps all soft modes at the same footing. This question has been explored in detail by Belitz *et al.* (2005). In practice, complications due to generic scale invariance are more common for quantum phase transitions than for classical ones because (i) there are more soft modes at $T = 0$ than at $T > 0$, and (ii) phenomena that classically only affects the dynamics influence the static critical behaviour of a quantum phase transition as well. In addition to this mechanism, there are other reasons for a quantum phase transition being more complicated than one might naively expect, including topological effects. In many of these cases, a description of the transition in terms of a Landau-Ginzburg-Wilson theory is not possible!

II. LANDAU'S FERMI LIQUID

In the last two decades a variety of metals have been discovered which display thermodynamic and transport properties at low temperatures which are fundamentally different from those of the usual metallic systems which are well descibed by the Landau Fermi-liquid theory. They have often been referred to as *Non-Fermi liquids*. We will see a very interesting example in Sec. III. A fundamental characteristic of such systems is that the low-evergy properties in a wide range of their phase diagram are dominated by singularities as a function of energy and temperature. Since these problems still relate to a liquid state of fermions, people sometimes call them *singular Fermi liquids (SFL)*.

The basic notions of Fermi-liquid theory have actually been with us at an intuitive level since the time of Sommerfeld: he showed that the linear low-temperature resistivity and optical conductivity could be understood by assuming that the electrons in a metal could be thought of as a gas of non-interacting fermions, i.e., in terms of quantum mechanical particles which do not have any direct interaction but which do obey Fermi statistics. Meanwhile, Pauli calculated that the paramagnetic susceptibility of non-interacting electrons is independent of temperature, also in accord with experiments in metals. At the same time it was understood, at least since the

work of Bloch and Wigner, that the interaction energies of the electrons in the metallic range of densities are not small compared to the kinetic energy. The rationalization for the qualitative success of the non-interacting model was provided by Landau, who initially was concerned with the properties of liquid ^{3}He. His work introduced a new way of thinking about the properties of interacting systems. The notion of quasiparticles and elementary excitations and the approach of asking useful questions about the low-energy excitations of the system based on concepts of symmetry, without worrying about the myriad unnecessary details, is encapsulated in Landau's phenomenological theory of Fermi liquids. The microscopic derivation of the theory was also soon developed.

The perspective on Fermi liquids has changed significantly in the last two decades. This is due both to changes of the theoretical perspective, and due to the experimental developments: on the experimental side, new materials have been found which exhibit Fermi-liquid behaviour in the temperature dependence of their low-temperature properties with the coefficients often a factor of order 10^3 different from the non-interacting electron values. These observations dramatically illustrate the power and range of validity of the Fermi-liquid ideas. On the other hand, new materials have been discovered whose properties are qualitatively different from the predictions of *Fermi-liquid theory (FLT)*. The most prominently discussed of these materials are the normal phase of high-temperature superconducting materials for a range of compositions near their highest T_c.

In this Section I will summarize some of the key features of Landau's FLT, without giving details which can be found in many of the classical textbooks, but instead focus on those elements of the theory that allows one to understand the possible routes by which the FLT can break down.

A. Essentials of Landau Fermi Liquids

The basic idea underlying Landau's Fermi-liquid theory (Landau, 1956) is that states with the same symmetry can be adiabatically connected. Simply put, this means that whether or not one can actually carry out the calculation, one knows that the eigenstates of the full Hamiltonian of the same symmetry can be obtained perturbatively from those of a simpler Hamiltonian. At the same time states of different symmetry cannot be obtained by "continuation" from the same state. This suggests that, given a tough problem which is impossible to solve, one may guess a right simple problem. The low-energy and long-wavelength excitations, as well as the correlation and the response functions of the tough problem bear a one-to-one correspondence with the simpler problem in their analytic properties. This leaves fixing only numerical values. These are to be determined by parameters, the minimum number of which is fixed by the symmetries. Experiments often provide an intuition

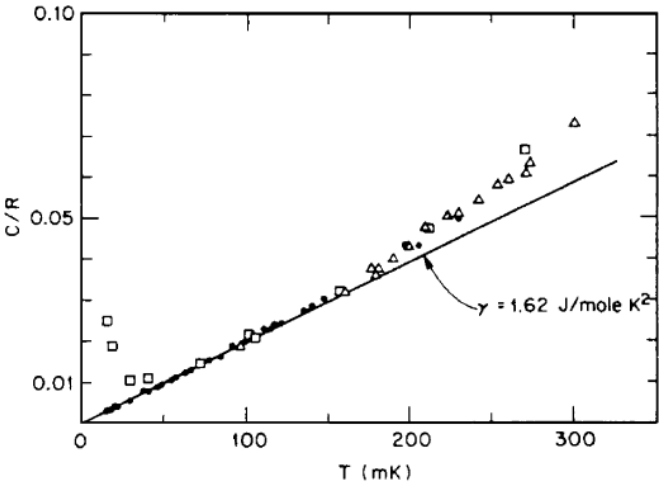

FIG. 3 Specific heat of $CeAl_3$ at low temperatures. The slope of the linear specific heat is about 3000 times that of the linear specific heat of, say, Cu. However, the high-temperature cutoff of this linear term is smaller than that of Cu by a similar amount. Figure from Andres *et al.* (1975).

as to what the right simple problem may be: for the interacting electrons, in the metallic range of densities, it is the problem of kinetic energy of particles with Fermi statistics. If one had started with the opposite limit, just the potential energy alone, the starting ground state is the Wigner crystal—a bad place to start thinking about a metal! If we start with non-interacting fermions, and then turn on the interactions, the qualitative behavior of the system does not change as long as the system does not go through (or is close to) a phase transition. Owing to the analyticity, one can even consider strongly interacting systems—the low-energy excitations in these have strongly renormalized values of their parameters compared to the non-interacting problem, but their qualitative behavior is the same as that of the simpler problem.

The heavy fermion problem provides an extreme example of the domain of validity of the Landau approach. This is illustrated in Fig. 3, which shows the specific heat of the heavy fermion compound $CeAl_3$.

As in the Sommerfeld model, the specific heat is linear in the temperature at low T, but if we write $C_v \approx \gamma T$ at low temperatures, the value of γ is about a thousand times as large as one would estimate from the density of states of a typical metal, using the free electron mass. For a Fermi gas, the density of states $N(0)$ at the Fermi energy is proportional to an effective mass $m^\star$

$$N(0) = \frac{m^\star k_F}{\pi^2 \hbar^2} \tag{2.1}$$

with k_F the Fermi wavenumber. Then the fact that the density of states at the chemical potential is a thousand times larger than for normal metals can be expressed by the statement that the effective mass $m^\star$ of the quasiparticles is a thousand times larger than the free electron mass m. Likewise, as Fig. 4 shows, the resistivity of

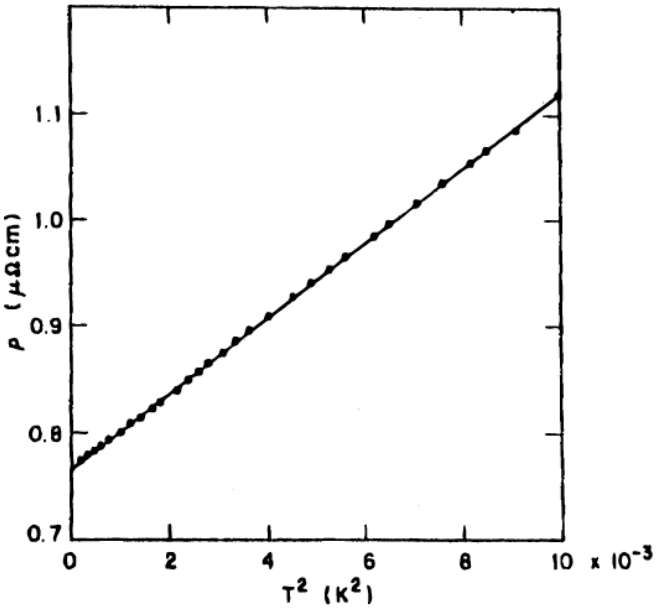

FIG. 4 Electrical resistivity of $CeAl_3$ below 100 mK, plotted against T^2. Figure from Andres *et al.* (1975).

$CeAl_3$ at low temperatures increases as T^2.

This also is a characteristic sign of a Fermi liquid, in which the quasiparticle lifetime τ at the Fermi surface, determined by electron–electron interactions, behaves as $\tau \sim 1/T^2$. However, just as the prefactor γ of the specific heat is a factor thousand times larger than usual, the prefactor of the T^2 term in the resistivity is a factor 10^6 larger—while γ scales linearly with the effective mass ratio $m^\star/m$, the prefactor of the T^2 term in the resistivity increases for this class of Fermi liquids as $(m^\star/m)^2$.

It should be remarked that the right simple problem is not always easy to guess. The right simple problem for liquid ^{4}He is not the non-interacting Bose gas but the weakly interacting Bose gas (the Bogoliubov problem).

For SFLs, the problem is different: usually one is in a regime of parameters where no simple problem is a starting point—in some cases the fluctuations between solutions to different simple problems determine the physical properties, while in others even this is lacking.

B. The Wavefunction Renormalization

Landau theory is the predecessor of the modern way of thinking about low-energy effective Hamiltonians in complicated problems and of the renormalization group.

Let us now consider the essential difference between non-interacting fermions and an interacting Fermi liquid from a simple microscopic perspective. For free fermions, the momentum states $|\boldsymbol{k}\rangle$ are also eigenstates of the Hamiltonian with eigenvalue

$$\varepsilon_{\boldsymbol{k}} = \frac{\hbar^2 k^2}{2m} \tag{2.2}$$

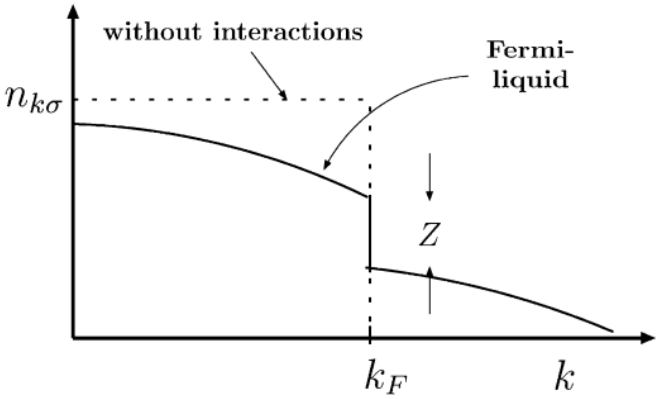

FIG. 5 Bare-particle distribution at $T = 0$ for a given spin direction in a translationally invariant Fermi system with interactions (full line) and without interactions (dashed line). The Fermi wavenumber k_F, is not renormalized by interactions! Figure from Varma *et al.* (2002).

Moreover, the thermal distribution of particles $n^0_{\boldsymbol{k}\sigma}$ is given by the Fermi–Dirac function, where σ denotes the spin label. At $T = 0$, the distribution jumps from 1 (all states occupied within the Fermi sphere) to zero (no states occupied within the Fermi sphere) at $|\boldsymbol{k}| = k_F$ and energy equal to the chemical potential μ. This is illustrated in Fig. 5.

A good way of probing a system is to investigate the *spectral function*; the spectral function $A(\boldsymbol{k}, \omega)$ gives the distribution of energies ω in the system when a particle with momentum $\boldsymbol{k}$ is added or removed from it (removing a particle below the Fermi energy means adding a hole).

As sketched in Fig. 6(a), for the non-interacting system, $A_0(\boldsymbol{k}, \omega)$ is simply a δ-function peak at the energy $\varepsilon_{\boldsymbol{k}}$, because all momentum states are also energy eigenstates ($\Im$ denotes the imaginary part of a complex function)

$$\begin{aligned} A_0(\boldsymbol{k}, \omega) &= \delta(\omega - (\varepsilon_{\boldsymbol{k}} - \mu)) \quad \text{for } \omega > \mu \\ &= -\frac{1}{\pi} \Im \frac{1}{\omega - (\varepsilon_{\boldsymbol{k}} - \mu) + i\delta} = -\frac{1}{\pi} \Im G^0(\boldsymbol{k}, \omega) \end{aligned}$$

Here, δ is small and positive; it means that particles or holes are introduced adiabatically, and it is taken to zero at the end of the calculation for the pure non-interacting problem. The first step of the second line is just a simple mathematical rewriting of the delta function. In the second line the Green's function G^0 for non-interacting electrons is introduced. More generally the single-particle Green's function $G(\boldsymbol{k}, \omega)$ is defined in terms of the correlation function of particle creation and annihilation operators in textbooks (Mahan, 1990). It is sufficient to note that it is related to the spectral function $A(\boldsymbol{k}, \omega)$, which has a clear physical meaning and which can be measured

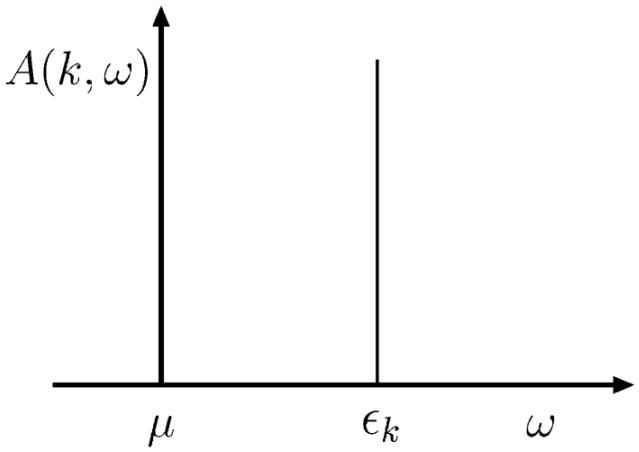

(a)The non-interacting spectral function $A(\boldsymbol{k},\omega)$ at fixed $\boldsymbol{k}$ as a function of ω.

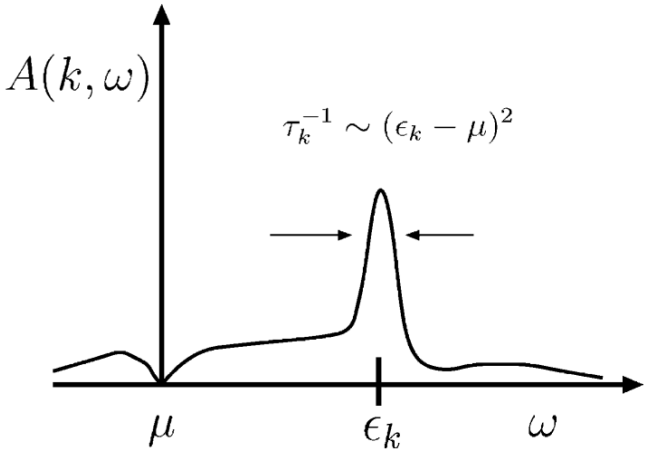

(b)The spectral function of single-electron excitations in a Fermi liquid at fixed $\boldsymbol{k}$ as a function of ω.

FIG. 6 If $(1/\pi)A(\boldsymbol{k},\omega)$ is normalized to 1 (one bare particle), the weight under the Lorentzian (the quasiparticle part) is Z. At the same time Z is the discontinuity in Fig. 5. Figure from Varma *et al.* (2002).

through angle-resolved photoemission experiments

$$G(\boldsymbol{k},\omega) = \int_{-\infty}^{\infty} dx \frac{A(\boldsymbol{k},x)}{\omega - \mu - x + i\,\delta\,\mathrm{sgn}(\omega-\mu)} \tag{2.3}$$

$A(\boldsymbol{k},\omega)$ thus is the spectral representation of the complex function $G(\boldsymbol{k},\omega)$. Here we have defined the so-called *retarded* Green's function which is especially useful since its real and imaginary parts obey the Kramers–Kronig relations. In the problem with interactions $G(\boldsymbol{k},\omega)$ will differ from $G^0(\boldsymbol{k},\omega)$. This difference can be quite generally defined through the single-particle self-energy function $\Sigma(\boldsymbol{k},\omega)$

$$(G(\boldsymbol{k},\omega))^{-1} = (G^0(\boldsymbol{k},\omega))^{-1} - \Sigma(\boldsymbol{k},\omega) \tag{2.4}$$

Eq. (2.3) ensures the relation between $G(\boldsymbol{k},\omega)$ and $A(\boldsymbol{k},\omega)$

$$A(\boldsymbol{k},\omega) = -\frac{1}{\pi}\Im G(\boldsymbol{k},\omega) \tag{2.5}$$

Let us now consider the form of $A(\boldsymbol{k},\omega)$ when we add a particle to an interacting system of fermions. Due to the interaction (assumed repulsive) between the added particle and those already in the Fermi sea, the added particle will kick particles from below the Fermi surface to above. The possible terms in a perturbative description of this process are constrained by the conservation laws of charge, particle number, momentum and spin.

Those which are allowed by these conservation laws are indicated pictorially in Fig. 7, and lead to an expression of the type

$$|\psi^{N+1}_{\boldsymbol{k}\sigma}\rangle = Z^{1/2}_{\boldsymbol{k}} c^\dagger_{\boldsymbol{k}\sigma}|\psi^N\rangle + \frac{1}{V^{3/2}} \sum_{\boldsymbol{k}_1,\boldsymbol{k}_2,\boldsymbol{k}_3} \sum_{\sigma_1,\sigma_2,\sigma_3} \alpha_{\boldsymbol{k}_1\sigma_1\boldsymbol{k}_2\sigma_2\boldsymbol{k}_3\sigma_3} c^\dagger_{\boldsymbol{k}_3} c_{\boldsymbol{k}_2} c^\dagger_{\boldsymbol{k}_1} \delta_{\boldsymbol{k},\boldsymbol{k}_1-\boldsymbol{k}_2+\boldsymbol{k}_3}\delta(\sigma;\sigma_1,\sigma_2,\sigma_3)|\psi^N\rangle + \ldots \tag{2.6}$$

Here the $c^\dagger_{\boldsymbol{k}}$'s and $c_{\boldsymbol{k}}$'s are the *bare* particle creation and annihilation operators, and the dots indicate higher-order terms, for which two or more particle–hole pairs are created and $\delta(\sigma;\sigma_1,\sigma_2,\sigma_3)$ expresses conservation of spin under vector addition. The multiple particle–hole pairs for a fixed total momentum can be created with a continuum of momenta of the individual bare particles and holes. Therefore, an added particle with fixed total momentum has a wide distribution of energies. However, if $Z_{\boldsymbol{k}}$ defined by Eq. (2.6) is finite, there is a well-defined feature in this distribution at some energy which is in general different from the non-interacting value $\hbar^2k^2/(2m)$. The spectral function in such a case will then be as illustrated in Fig. 6(b). It is useful to separate the well-defined feature from the broad continuum by writing the spectral function as the sum of two terms, $A(\boldsymbol{k},\omega) = A_{\rm coh}(\boldsymbol{k},\omega) + A_{\rm incoh}(\boldsymbol{k},\omega)$. The single-particle Green's function can similarly be expressed as a sum of two cor-

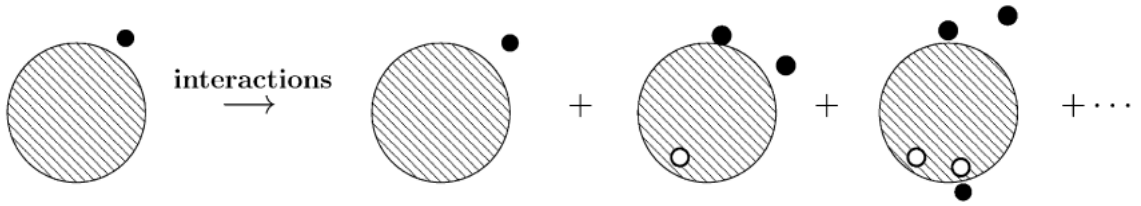

FIG. 7 Schematic illustration of the perturbative expansion (2.6) of the change of wavefunction as a result of the addition of an electron to the Fermi sea due to interactions with the particles in the Fermi sea. Figure from Varma *et al.* (2002).

responding terms, $G(\boldsymbol{k},\omega) = G_{\rm coh}(\boldsymbol{k},\omega) + G_{\rm incoh}(\boldsymbol{k},\omega)$. Then

$$G_{\rm coh}(\boldsymbol{k},\omega) = \frac{Z_{\boldsymbol{k}}}{\omega - \tilde{\varepsilon}_{\boldsymbol{k}} + i/\tau_{\boldsymbol{k}}} \tag{2.7}$$

which for large lifetimes $\tau_{\boldsymbol{k}}$ gives a Lorentzian peak in the spectral density at the quasiparticle energy $\tilde{\varepsilon}_{\boldsymbol{k}} \equiv \varepsilon_{\boldsymbol{k}} - \mu$. The incoherent Green's function is smooth and hence for large $\tau_{\boldsymbol{k}}$ corresponds to the smooth background in the spectral density.

The condition for the occurrence of the well-defined feature can be expressed as the condition that the self-energy $\Sigma(\boldsymbol{k},\omega)$ has an analytic expansion about $\omega = 0$ and $\boldsymbol{k} = \boldsymbol{k}_F$ and that its real part is much larger than its imaginary part. One can easily see that, if this was not true, then expression (2.7) for $G_{\rm coh}$ could not be obtained. These conditions are necessary for a Landau Fermi liquid. Upon expanding $\Sigma(\boldsymbol{k},\omega)$ for small ω and small deviations of $\boldsymbol{k}$ from $\boldsymbol{k}_F$ and writing it in the form (2.7), one can make the identifications (in what follows, v_F and E_F denote the Fermi velocity and energy, respectively)

$$\tilde{\varepsilon}_{\boldsymbol{k}} = \varepsilon_{\boldsymbol{k}} Z_{\boldsymbol{k}} \hat{Z}_{\boldsymbol{k}}, \quad \frac{1}{\tau_{\boldsymbol{k}}} = -Z_{\boldsymbol{k}} \Im\Sigma(\boldsymbol{k}_F, \omega = 0) \tag{2.8}$$

where

$$\begin{aligned} Z_{\boldsymbol{k}} &= \left(1 - \frac{\partial\Sigma}{\partial\omega}\right)^{-1}_{\omega=0,\boldsymbol{k}=\boldsymbol{k}_F} \\ \hat{Z} &= \left(1 + \frac{1}{v_F}\frac{\partial\Sigma}{\partial\boldsymbol{k}}\right)_{\omega=0,\boldsymbol{k}=\boldsymbol{k}_F} \end{aligned} \tag{2.9}$$

From Eq. (2.6), we have a more physical definition of $Z_{\boldsymbol{k}}$: it is the projection amplitude of $|\psi^{N+1}_{\boldsymbol{k}}\rangle$ onto the state with one bare particle added to the ground state, since all other terms in the expansion vanish in the thermodynamic limit in the perturbative expression of Eq. (2.6)

$$Z^{1/2}_{\boldsymbol{k}} = \langle\psi^{N+1}_{\boldsymbol{k}}|c^\dagger_{\boldsymbol{k}}|\psi^N\rangle \tag{2.10}$$

In other words, $Z_{\boldsymbol{k}}$ is the overlap of the ground state wavefunction of a system of $N \pm 1$ interacting fermions of total momentum $\boldsymbol{k}$ with the wavefunction of N interacting particles and a bare particle of momentum $\boldsymbol{k}$. $Z_{\boldsymbol{k}}$ is called the *quasiparticle amplitude*.

The Landau theory assumes that $Z_{\boldsymbol{k}}$ is finite. It also states that for small ω and $\boldsymbol{k}$ close to $\boldsymbol{k}_F$, the physical properties can be calculated from quasiparticles which carry the same quantum numbers as the particles, i.e., charge, spin and momentum and which may be defined simply by the creation operator $\gamma^\dagger_{\boldsymbol{k},\sigma}$

$$|\psi^{N+1}_{\boldsymbol{k}}\rangle = \gamma^\dagger_{\boldsymbol{k},\sigma}|\psi^N\rangle \tag{2.11}$$

Close to $\boldsymbol{k}_F$, and for T small compared to the Fermi energy, the distribution of the quasiparticles *is assumed to be the Fermi–Dirac distribution* in terms of the renormalized quasiparticle energies. The bare particle distribution is quite different. As is illustrated in Fig. 5, it is depleted below $\boldsymbol{k}_F$ and increased above $\boldsymbol{k}_F$, with a discontinuity at $T = 0$, whose value is shown in microscopic theory to be $Z_{\boldsymbol{k}}$. A central result of Fermi liquid theory is that close to the Fermi energy at zero temperature, the width $1/\tau_{\boldsymbol{k}}$ of the coherent quasiparticle peak is proportional to $(\tilde{\varepsilon}_{\boldsymbol{k}} - \mu)^2$, so that near the Fermi energy the lifetime is long and quasiparticles are well-defined. At the Fermi energy, $1/\tau_{\boldsymbol{k}}$ varies with temperature as T^2. From the microscopic derivation of this result, it follows that the weight in this peak, $Z_{\boldsymbol{k}}$, becomes equal to the jump Z in $n_{\boldsymbol{k}\sigma}$ when one approaches the Fermi surface: $Z_{\boldsymbol{k}} \to Z$ for $\boldsymbol{k} \to \boldsymbol{k}_F$. For heavy fermions, as I already mentioned, Z can be of the order of 10^{-3}. However, as long as Z is non-zero, one has Fermi liquid properties for temperatures lower than about ZE_F. Degeneracy is effectively lost for temperatures much higher than ZE_F and classical statistical mechanics takes over.

An additional result from microscopic theory is the so-called *Luttinger theorem*, which states that the volume enclosed by the Fermi surface does not change due to interactions (Mahan, 1990). The mathematics behind this theorem is that with the assumptions of FLT, the number of poles in the interacting Green's function below the chemical potential is the same as that for the non-interacting Green's function (which just the number of particles in the system).

Landau actually started his discussion of the Fermi liquid by writing the equation for the deviation of the free energy from its ground state value as a functional of the deviation of the quasiparticle distribution function $n(\boldsymbol{k},\sigma)$ from the equilibrium distribution function $n_0(\boldsymbol{k},\sigma)$

$$\delta n(\boldsymbol{k},\sigma) = n(\boldsymbol{k},\sigma) - n_0(\boldsymbol{k},\sigma) \tag{2.12}$$

as follows

$$G = G_0 + \frac{1}{V}\sum_{\boldsymbol{k},\sigma}(\tilde{\varepsilon}_{\boldsymbol{k}} - \mu)\delta n_{\boldsymbol{k}\sigma} + \frac{1}{2V^2}\sum_{\boldsymbol{k}\boldsymbol{k}',\sigma\sigma'} f_{\boldsymbol{k}\boldsymbol{k}',\sigma\sigma'}\delta n_{\boldsymbol{k}\sigma}\delta n_{\boldsymbol{k}'\sigma'} + \ldots \tag{2.13}$$

Note that $(\tilde{\varepsilon}_{\boldsymbol{k}} - \mu)$ is itself a function of δn; so the first term contains at least a contribution of order $(\delta n)^2$ which makes the second term quite necessary. In principle, the unknown function $f_{\boldsymbol{k}\boldsymbol{k}',\sigma\sigma'}$ depends on spin and momenta. However, spin rotation invariance allows one to write the spin part in terms of two quantities, the symmetric and antisymmetric parts $f^{\rm s}$ and $f^{\rm a}$. Moreover, for low energy and long-wavelength phenomena only momenta with $\boldsymbol{k} \approx \boldsymbol{k}_F$ play a role; if one considers the simple case of ^{3}He where the Fermi surface is spherical, rotation invariance implies that, for momenta near the Fermi momentum, f can only depend on the relative angle between $\boldsymbol{k}$ and $\boldsymbol{k}'$; this allows one to expand in Legendre polynomials $P_l(x)$ by writing

$$N(0) f^{\rm s,a}_{\boldsymbol{k}\boldsymbol{k}',\sigma\sigma'} \xrightarrow{\boldsymbol{k}\approx\boldsymbol{k}'\approx\boldsymbol{k}_F} \sum_{l=0}^{\infty} F_l^{\rm s,a} P_l(\hat{\boldsymbol{k}}\cdot\hat{\boldsymbol{k}}') \tag{2.14}$$

From expression (2.13) one can then relate the lowest order so-called *Landau coeffcients* F_0 and $F_1^{\rm s}$ and the effective mass $m^\star$ to thermodynamic quantities like the specific heat C_v, the compressibility κ, and the susceptibility χ

$$\frac{C_v}{C_{v0}} = \frac{m^\star}{m}, \quad \frac{\kappa}{\kappa_0} = (1+F_0^{\rm s})\frac{m^\star}{m}, \quad \frac{\chi}{\chi_0} = (1+F_0^{\rm a})\frac{m^\star}{m}$$

Here, subscript 0 refers to the quantities of the non-interacting reference system, and m is the mass of the fermions. For a Galilean invariant system (like ^{3}He), there is a simple relation between the mass enhancement and the Landau parameter $F_1^{\rm s}$, and there is no renormalization of the particle current $\boldsymbol{j}$; however, there *is* a renormalization of the velocity

$$\boldsymbol{j} = \frac{\boldsymbol{k}}{m}, \quad \boldsymbol{v} = \frac{\boldsymbol{k}}{m^\star}, \quad \frac{m^\star}{m} = \left(1 + \frac{F_1^{\rm s}}{3}\right) \tag{2.15}$$

The transport properties are calculated by defining a distribution function $\delta n(\boldsymbol{k}\sigma; r, t)$ which is slowly varying in space and time and writing a Boltzmann equation for it.

It is a fact of the Landau theory that the expressions of the low-energy properties in terms of the quasiparticles in no place involve the quasiparticle amplitude $Z_{\boldsymbol{k}}$. In fact, in a translationally invariant problem such as liquid ^{3}He, $Z_{\boldsymbol{k}}$ cannot be measured by any thermodynamic or transport measurements. A good use of conservation laws ensures that Z's cancel out in all physical properties. This is no longer true on a lattice, in heavy fermions (Varma, 1985), or in any situation where the interacting problem contains more than one type of particle with different characteristic frequency scales.

C. Routes to Breakdown of Landau Theory

From Landau's phenomenological theory, one can only say that the theory breaks down when the physical properties—specific heat, compressibility, or the magnetic susceptibility—diverge or when the collective modes representing oscillations of the Fermi surface in any harmonic and singlet/triplet spin combinations become unstable.

The discussion following Eq. (2.6) in Section II.B allows one to make a more general statement. Landau theory breaks down when the quasiparticle amplitude $Z_{\boldsymbol{k}}$ becomes zero; i.e., when the states $c^\dagger_{\boldsymbol{k}}|\psi^N\rangle$ and $|\psi^{N+1}_{\boldsymbol{k}}\rangle$ are orthogonal. This can happen if the series expansion in Eq. (2.6) in terms of the number of particle–hole pairs is divergent. In other words, the addition of a particle or a hole to the system creates a divergent number of particle–hole pairs in the system so that the leading term does not have a finite weight in the thermodynamic limit. From Eq. (2.9), which links the Z's to Σ's, this requires the single-particle self-energy to be singular as a function of ω at $\boldsymbol{k} \simeq \boldsymbol{k}_F$. This in turn means that the Green's functions of SFLs contain branch cuts rather than poles, unlike Landau Fermi liquids. The weakest singularity of this kind is encountered in the so-called "marginal Fermi liquids", where

$$\Sigma(\boldsymbol{k}_F, \omega) \simeq \lambda\left[\omega \ln\frac{\omega_c}{\omega} + i|\omega|\right] \tag{2.16}$$

To see why this is the marginal case, note that a requisite for the definition of a quasiparticle is that the quasiparticle peak width $\tau^{-1}_{\boldsymbol{k}} = 2\Sigma''$ should vanish faster than linear in ω, the quasiparticle energy. Thus, $\Sigma'' \sim \omega$ is the first power for which this is not true. The $\omega\ln(\omega_c/\omega)$ term in Eq. (2.16) is then dictated by the Kramers–Kroning relation.

If a divergent number of low-energy particle–hole pairs is created upon the addition of a bare particle, it means that the low-energy response functions (which all involve creating particle–hole pairs) of SFLs are also divergent. The implication is that the interaction vertices are actually more divergent than the single-particle self-energy.

Another route to SFLs is the case in which the interactions generate new quantum numbers which are not descriptive of the non-interacting problem. This happens in particular in the Quantum Hall problems as well as in problems of impurity scattering with special symmetries. In such cases, the new quantum numbers characterize new low-energy topological excitations. New quantum numbers of course imply $Z = 0$, but does $Z = 0$ imply new quantum numbers? One might wish to conjecture that this is so. However, no general arguments on this point are available.

Ultimately, all breakdowns of Landau theory are due to degeneracies leading to singular low-energy fluctuations. If the characteristic energy of the fluctuations is lower than the temperature, a quasi-classical statistical mechanical problem results. One may divide the various

routes to breakdown of Landau theory into the following classes:

(i) *Landau–Pomeranchuk singularities*: Landau theory points to the possibility of its breakdown through the instability of the collective modes of the Fermi-surface. These collective modes can be characterized by the angular momentum l of oscillation of the Fermi surface and whether the oscillation is symmetric "s" or antisymmetric "a" in spin. The condition for the instability derived from the condition of zero frequency of the collective modes is (Baym and Pethick, 1991; Pines and Nozieres, 1990)

$$F_l^{\rm s} \leqslant -(2l+1), \quad F_l^{\rm a} \leqslant -(2l+1) \tag{2.17}$$

The $l = 0$ conditions refer to the divergence in the compressibility and the spin susceptibility. The former would in general occur via a first-order transition. The latter describes the ferromagnetic instability. No other Landau–Pomeranchuk instabilities have been experimentally identified.

(ii) *Critical regions of large Q-singularities*: Landau theory concerns itself only with long-wavelength response and correlations. A Fermi liquid may have instabilities at a non-zero wavevector, for example a charge-density wave (CDW) or spin-density wave (SDW) instability. Only a microscopic calculation can provide the conditions for such instabilities and therefore such conditions can only be approximately derived. An important point to note is that they arise perturbatively from repeated scattering between the quasiparticle parts of G. The superconductive instability for any angular momentum is also an instability of this kind. In general, such instabilities are easily seen in random-phase approximation calculations.

Singular Fermi liquid behavior is generally expected to occur only in the critical regime of such instabilities. If the transition temperature T_c is finite then there is usually a stable low-temperature phase in which unstable modes are condensed to an order parameter, translational symmetry is broken, and gaps arise in part or all of the Fermi surface. For excitations on the surviving part of the Fermi surface, Fermi-liquid theory is usually again valid. The fluctuations in the critical regime are classical, with characteristic frequency $\omega_{\rm FL} \ll k_B T_c$.

If the transition is tuned by some external parameter so that it occurs at zero temperature, one obtains, as illustrated already in Fig. 2, a quantum critical point (QCP). If the transition is approached at $T = 0$ as a function of the external parameter, the fluctuations are quantum-mechanical, while if it is approached as a function of temperature for the external parameter at its critical value, the fluctuations have a characteristic energy proportional to the temperature. A large region of the phase diagram near QCPs often carries SFL properties.

(iii) *Special symmetries*: The Cooper instability at $q = 0$ is due to the *nesting* of the Fermi surface in the particle–particle channel. Usually, indications of finite-q CDW or SDW singularities are evident pertubatively for special Fermi surfaces, nested in some $\boldsymbol{q}$-direction in particle–hole channels. One-dimensional fermions are perfectly nested in both particle–hole channels and particle–particle channels and hence they are both logarithmically singular. Pure one-dimensional fermions also have the extra conservation law that right going and left going momenta are separately conserved. These introduce special features to the SFL of one-dimensional fermions, such as extra quantum numbers. Several soluble impurity problems with special symmetries have SFL properties.

(iv) *Long-range interactions*: The breakdown of Landau Fermi liquid may come about through long-range interactions, either in the bare Hamiltonian through the irreducible interaction or through a generated effective interaction. The latter, of course, occurs in the critical regime of phase transitions as discussed above. Coulomb interactions will not work for the former, because of screening of charge fluctuations.

III. THE ITINERANT-ELECTRON FERROMAGNET MnSi

MnSi is one of the most extensively studied of the itinerant-electron ferromagnets. (In this context, *itinerant* means "free to move"–as opposed to bound–electrons.) The ordering temperature of MnSi is $T_c = 29.5$ K at ambient pressure and it vanishes above a critical pressure, p_c, of only 14.6 kbar.

The normal state of itinerant-electron ferromagnets such as Fe, Ni and Co could be described in terms of the standard model of the metallic state or its extension know as the *nearly ferromagnetic Fermi liquid theory* (NFFL) (Stoner, 1938). In recent years, however, a large number of observations has accumulated from various complex intermetallic systems (Varma *et al.*, 2002) that raises the possibility that this assumption might be wrong.

Pfleiderer *et al.* (2001) have examined this issue by means of high-precision measurements of the electrical transport and magnetic properties of MnSi. They tuned the Curie temperature towards absolute zero by the application of hydrostatic pressure. These measurements revealed a striking combination of properties–most notably a $T^{3/2}$ power law dependence of the resistivity.

In this Section we will see some of the recent experimental data available on MnSi, and then some theoretical results.

A. Experimental data on MnSi

1. Resistivity and Neutron Scattering Measurements

MnSi crystallizes in the cubic B20 structure shown in Fig. 8.

This structure is somewhat unusual in that it lacks strict space-inversion symmetry. This may be suppressing superconductivity that would otherwise be expected to arise on the border of itinerant-electron ferromagnetism (Pfleiderer, 2001a). This gives one the opportunity to track the normal metallic state of interest near

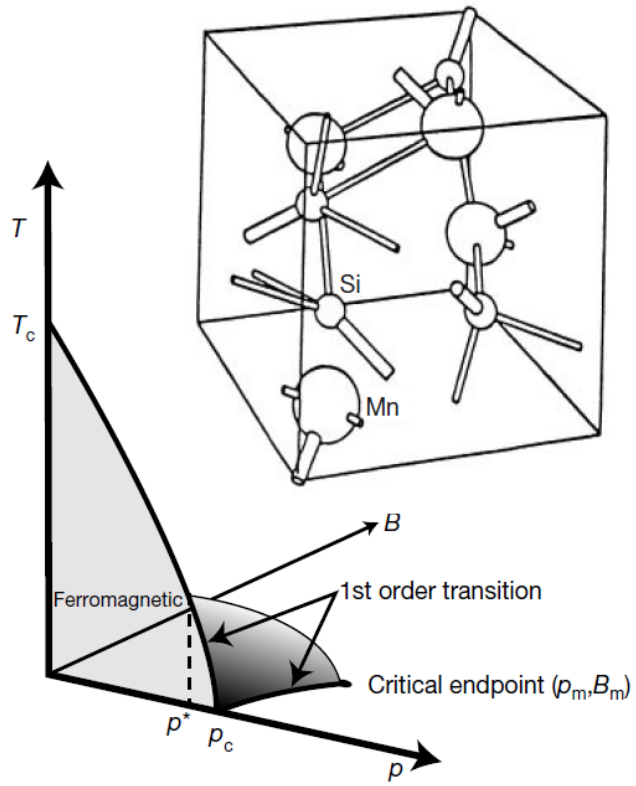

FIG. 8 Diagram of the ferromagnetic state of MnSi and its crystallographic structure. In the temperature-pressure (T-p) plane ($B = 0$) the transition drops with increasing pressure from its ambient pressure value of $T_c = 29.5$ K and changes from second to weakly first order at $p^\star = 12$ kbar where $T_c \approx 12$ K before it dissapears above $p_c = 14.6$ kbar. In the magnetic field-pressure (B-p) plane ($T = 0$) the transition is weakly first-order up to a critical endpoint, estimated to be at $B_m = 0.6$ T and $p_m = 17$ kbar. In the dome on the left MnSi is ordered ferromagnetically. The inset shows the crystallographic unit cell of the B20 crystal structure of MnSi. Figure from Pfleiderer *et al.* (2001).

p_c over five orders of magnitude in temperature, from below 10 mK to room temperature, in an ultra-pure system without intervening phase transitions.

In the phase diagram of temperature versus pressure and field, the Curie temperature, T_c, in MnSi falls monotonically with pressure, p, and magnetic field, B, as shown in Fig. 8. The transition is second-order along the zero-field axis up to $p^\star \approx 12$ kbar where $T_c \approx 12$ K and along the contour at finite fields terminating at the point ($p_m \approx 17$ kbar, $B_m \approx 0.6$ T) where T_c vanishes. The transition is, however, weakly first-order within a cavity extending to finite fields, and in particular between $p^\star$ and p_c where T_c falls to zero along the zero-field axis. For a fixed field, a first-order line in the B-p plane is seen to end in a second-order point in a way which is reminiscent of a conventional liquid-gas transition in the van der Waals model. At B_m this line collapses to a single point that represents a second-order transition with zero T_c. This type of phase diagram has been observed in several related materials (Goto *et al.*, 1997; Huxley *et al.*, 2000) and theoretical considerations suggest that it may be generally valid for itinerant-electron ferromagnets in the limit $T_c \to 0$.

A crucial aspect is the temperature dependence of the electrical resistivity in the p-B region of the phase diagram just outside the dome in which magnetic order is found. The main result of (Pfleiderer *et al.*, 2001) is that the resistivity in this region exhibits a temperature dependence of the form $\rho(T) = \rho_0 + AT^{3/2}$ over a remarkably wide range (in temperature) of nearly three orders of magnitude. An example of this striking behaviour is shown in Figs. 9 and 11 for a pressure just above p_c, in zero magnetic field, and for a very pure sample. This behaviour extends also up to the boundary of ferromagnetism as a function of field for pressures close to (but above) p_c.

The $T^{3/2}$ coefficient, A, is only weakly dependent on ρ_0, but it is sensitive to pressure and falls by approximately a factor of 2 from p_c to $2p_c$.

The "conventional" T^2 form of the resistivity is observed in MnSi only at low temperatures in (1) the ferromagnetic state and (2) the normal state at pressures far above p_c.

Pfleiderer (2004) reported neutron scattering measurements of MnSi, revealing that sizeable quasi-static magnetic moments survive far into the non-Fermi liquid phase. These moments are organized in an unusual pattern with partial long-range order. Their observation supports the existence of novel metallic phases with partial ordering of the conduction electrons (reminescent of liquid crystals).

Shown in Fig. 10 is a qualitative illustration of this key result. Below a crossover temperature T_0 and even for pressures well above p_c (deep inside the NFL phase), they observed static magnetic order. This alone is unexpected, because the bulk properties clearly suggest the loss of long-range order at p_c. Moreover, instead of well-defined magnetic Bragg satellites, scattering intensity is found essentially everywhere on the surface of a tiny sphere. The total integrated scattering intensity over the sphere at 1.6 K is of similar magnitude to that at ambient pressure. This is consistent with the observation that the bulk magnetic moment is almost independent of pressure in a polarizing magnetic field of 0.6 T, and suggests that one is seeing the dominant feature of the magnetic state at high pressure.

2. Comparison with NFFL Predictions

In the search for a possible explanation of the $T^{3/2}$ power law, Pfleiderer and co-workers have considered the predictions of a theoretically well established extension of the Fermi-liquid picture, namely the nearly ferromagnetic Fermi-liquid (NFFL) model.

The behaviour of the NFFL model depends on the temperature scales $T^\star = T_F/(k_F \xi S)$, where T_F is the

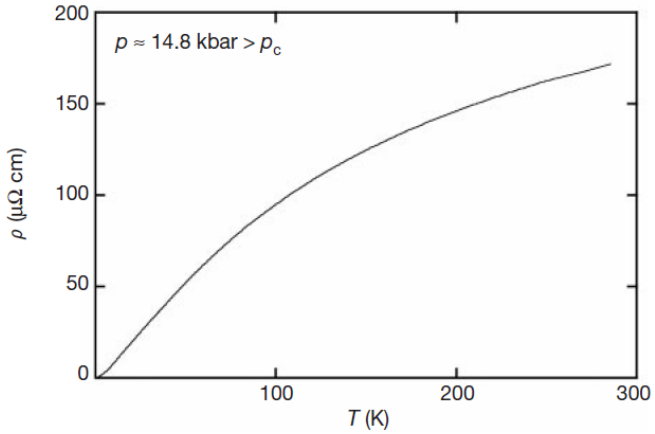

(a)The resistivity on a linear T scale below room temperature. $\rho(T)$ drops monotonically from a high T value by nearly three orders of magnitude and changes from a sublinear to a superlinear dependence below roughly 15 K.

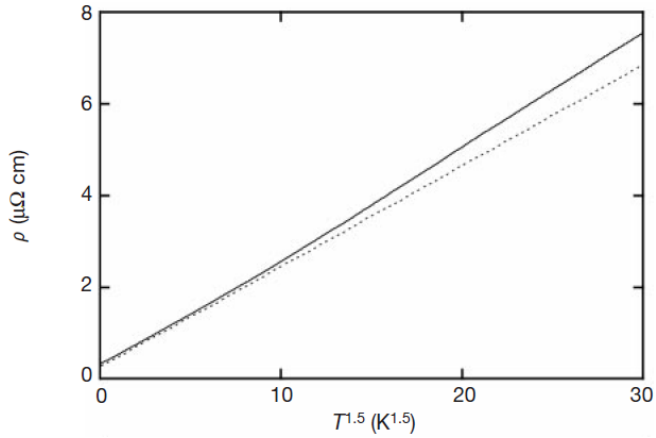

(b)The resistivity on a $T^{3/2}$ scale below 10 K. Below 5 K a $T^{3/2}$ dependence is observed, where the T-dependent part is large compared to ρ_0. Dotted line represents a $T^{3/2}$ behaviour.

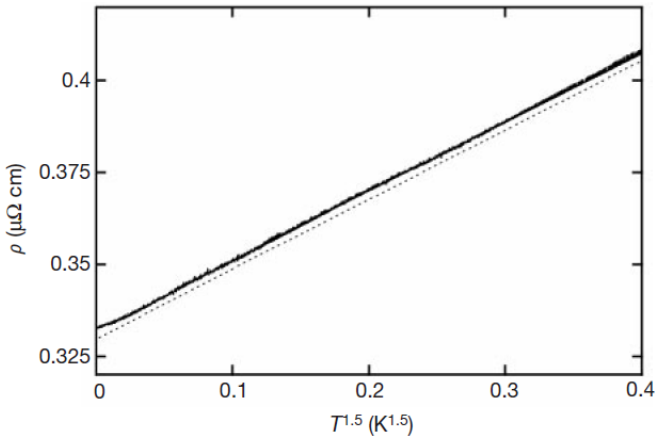

(c)The resistivity on a $T^{3/2}$ scale below 0.5 K. A $T^{3/2}$ dependence is observed down to the lowest T investigated, where the T-dependent part is small compared to ρ_0. Dotted line represents a $T^{3/2}$ behaviour.

FIG. 9 Temperature dependence of the resistivity $\rho(T)$ of MnSi above the critical pressure in different T regimes. Figure from Pfleiderer *et al.* (2001).

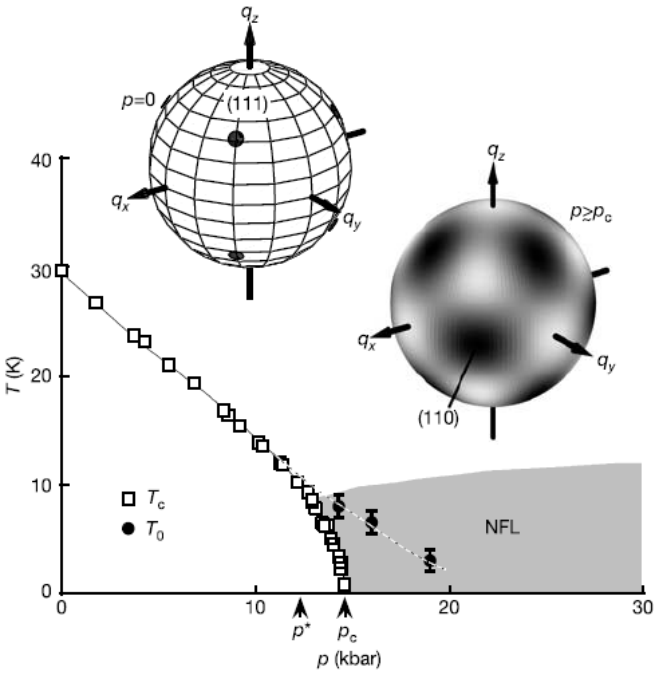

FIG. 10 Schematic temperature T versus pressure p phase diagram of MnSi, and qualitative illustration of the scattering intensity characteristic of the magnetic state. The insets qualitatively show the location and key features of elastic magnetic scattering intensity in reciprocal space at ambient pressure (left) and at high pressure (right). Data were collected near the [110] lattice Bragg peak. At ambient pressure, resolution-limited magnetic Bragg peaks (indicated by the black dots) are observed at a distance $Q = 0.037$ Å^{-1}, characteristic of three-dimensional long-range magnetic order. At high pressure, intensity is observed below a crossover temperature T_0 on the surface of a tiny sphere of radius $Q \approx 0.043$ Å^{-1}. The intensity on this surface varies as roughly depicted by the shading, and is highest around ⟨110⟩. Figure from Pfleiderer (2004).

Fermi temperature, k_F is the Fermi wavevector, ξ is the magnetic correlation length and S is the Stoner enhancement factor (the ratio of the magnetic susceptibility with and without exchange enhancement). For temperatures well below $T^\star$, the NFFL model reduces to the Fermi-liquid model discussed in Section II, which is characterized by a T^2 resistivity, as already noted. Above $T^\star$, the NFFL model reduces to the so-called *marginal Fermi-liquid model* (Millis, 1993), which is characterized by a $T^{5/3}$ resistivity when T is far below T_F for a three-dimensional system and for a dominance of small-angle electron scattering in the electronic transport. When the latter assumption breaks down, $\rho(T)$ is expected to be linear in T.

A comparison of the prediction of the NFFL model with experiment is shown in Fig. 11. At p_c and zero magnetic field, $T^\star$ for MnSi is consistent within a few K with the first-order nature of T_c just below p_c. The resistivity exponent is thus expected to be described by the marginal Fermi-liquid model above 5 K, but by Fermi-

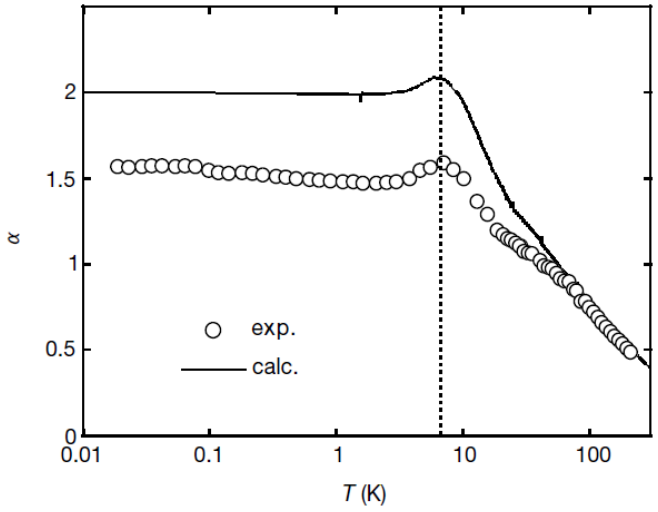

FIG. 11 Comparison of the experimentally observed temperature dependence of the resistivity above $p_c = 14.6$ kbar with NFFL predictions. The power-law exponent α, extracted from $\Delta\rho(T) \propto T^{\alpha}$, versus temperature on a logarithmic scale. The experimentally observed exponent crosses from the high-T to the low-T regime around 15 K. Below several kelvin it locks to a $T^{3/2}$ dependence over nearly three orders of magnitude in T. The expected behaviour in the NFFL model evaluated for MnSi predicts a T^2 dependence below a few kelvin. Note that the crossover towards the high-T behaviour is predicted correctly, in contrast with the qualitative $T^{3/2}$ form at low T, which is radically different. Figure from Pfleiderer *et al.* (2001).

liquid theory in the millikelvin range. As shown in Fig. 11, the NFFL model does indeed agree with experiment above a few kelvin, but is seen to break down dramatically at lower temperatures where the unexpected $T^{3/2}$ power law prevails.

The $T^{3/2}$ power law qualitatively corresponds to the effects of frozen-in disorder, as observed, for example, in amorphous metals and polycrystalline spin glasses (Ford and Mydosh, 1976), which are expected to lead to a diffusive motion of charge carriers on length scales substantially larger than the mean free path (Fischer, 1979; Rivier and Mensah, 1977). But the samples investigated by Pfleiderer *et al.* (2001) have mean free paths of the order of 5000 Å! So, only well below a new temperature scale $T_F/(k_F l)$ is it possible that a $T^{3/2}$ term in the resistivity may arise. This scale, however, is at least an order of magnitude too small to explain the range of the $T^{3/2}$ resistivity shown in Figs. 9 and 11. Apart from this, the impurity model would also seem to be at odds with the observed weak dependence of A on ρ_0.

B. Theoretical Modelling

1. Skyrmions

Skyrme was the first to succeessfully describe nuclear particles as localized states, so-called 'skyrmions' (Skyrme, 1961). Skyrmionic states have been found under non-equilibrium conditions, or when stabilized by external fields or the proliferation of topological defects. Examples are spin textures in quantum Hall magnets or the blue phases in liquid crystals. However, it has generally been assumed that skyrmions cannot form spontaneous ground states, such as ferromagnetic or antiferromagnetic order, in magnetic materials. Spontaneous skyrmion ground states were not considered to be stable, and people assumed they could only be induced by an appropriate applied field or the proliferation of topological defects.

Inspired by the recent discovery of a non-Fermi liquid phase and partial magnetic order in the cubic itinerant-electron helimagnet MnSi (Section III.A), Roszler *et al.* (2006) have shown that this assumption is wrong and that *skyrmion textures may form spontaneously in condensed-matter systems with chiral interactions without the assistance of external fields or the proliferation of defects.* They used a phenomenological continuum model based on a few material-specific parameters that can be determined experimentally. The main difference from previous models is the allowance for softened amplitude variations of the magnetization. Spontaneous skyrmion ground states may exist generally in materials with *chiral interactions.* Chiral interactions are present in many different systems, such as (1) spin-orbit interactions in non-centrosymmetric materials, also referred to as Dzyaloshinsky–Moriya interactions (2) in non-centrosymmetric ferroelectrics, (3) in chiral liquid crystals etc.

Roszler and co-workers have considered systems with a hierachy of well-separated energy and length scales, where ferromagnetic exchange favouring spin alignment is the strongest scale, followed by chiral interactions favouring spin rotations on intermediate scales, and magnetic anisotropies and dipolar interactions that determine favourable directions of spins as the weakest scale.

The magnetic free energy density is written in the form

$$f = Am^2 \sum_{i,j} (\partial_i n_j)^2 + \eta A (\nabla m)^2 + f_D(\boldsymbol{m}) + f_0(m) \quad (3.1)$$

where the first and second term in A and ηA (where η, $A > 0$), respectively, describe the *magnetic stiffness*, with $\boldsymbol{n}$ being a unit vector along the magnetization, $\boldsymbol{m} = m\boldsymbol{n}$. The gradient terms describe additional softening of the amplitude of the magnetization for $\eta < 1$. The third term $f_D(\boldsymbol{m}) \equiv D\mathcal{L}(\boldsymbol{m})$ in the free energy describes the chiral interactions, where the Dzyaloshinsky–Moriya constant D determines its handedness and strength. The Dzyaloshinsky–Moriya interactions can be expressed in terms of so-called Lifshitz

invariants (linear, antisymmetric gradient terms of the magnetization) $\mathcal{L}_{ij}^{(k)} = (m_i\partial_k m_j - m_j\partial_k m_i)$, where i, j, k are combinations of cartesian coordinates x, y, z that are consistent with the symmetry class of the system under consideration. The fourth term $f_0(m)$ includes non-gradient terms of the free energy and may be expanded according to Landau theory in even powers of m (see Section I.A).

Expanding the contribution $f_0(m)$ according to Landau theory for small values of m as $f_0 = a(T - T_c)m^2 + bm^4 + \ldots$ leads, in the absence of chiral interactions ($f_D = 0$), to the conventional Curie temperature T_c of centrosymmetric systems. Thus, when the temperature drops below T_c, the energy density of a ferromagnetically spin-aligned state is lowest. Chiral interactions ($f_D < 0$) favouring rotations of the moments with respect to each other reduce the energy density further. This stabilization of twisted magnetic states occurs only by the competition of the Dzyaloshinsky–Moriya interactions with the exchange, expressed by the form of the gradient energy. Therefore, the exact form of $f_0(m)$ is not decisive for the stability of skyrmions.

Figure 12 illustrates the twisted magnetic structures with rotating magnetization and Fig. 13 the associated energy densities. For rotations along a single given direction, shown in Fig. 12(a), the reduction in energy density, shown in Fig. 13, is uniform. Therefore, the transition to the ferromagnetic state is replaced by a transition to a one-dimensionally modulated state at a temperature (the unit length used throughout this Section is $1/q_0$, which is the inverse of the twisting length in chiral magnets with Dzyaloshinsky–Moriya couplings; energy and temperature are given in quivalent units of $D^2/(2Aa)$)

$$T_h = T_c + \frac{D^2}{4Aa} \tag{3.2}$$

As shown in Figs. 12(b) and 13, rotations of the magnetization in two dimensions reduce the energy density even further near its nucleation point at the centre of the cylindrical structure $\rho = 0$. Considering only the energy reduction at $\rho = 0$, one obtains an upper limit for the temperature T_D for the onset of this so-called *double-twisting*:

$$T_D = T_c + \frac{D^2}{2Aa} \tag{3.3}$$

The ratio A/D measures the pitch of the chiral modulations in the ordered helical state, while D/a measures the chirality of magnetic fluctuations in the paramagnetic state. Hence, D/a is related to a chiral component of the susceptibility. The parameters a and b are the initial susceptibility and mode coupling parameter, respectively. This permits estimates of T_h and T_D from experiments.

As seen in Fig. 13, the energy reduction due to a double-twist is no longer uniform. In fact, for fixed magnetization amplitude the energy reduction turns into an excess of the energy density at larger distances ρ from the centre, which outweighs the initial reduction. This destabilizes the double-twist structure altogether, which is the reason why magnetic skyrmions were believed to be unstable. Skyrmion textures may only form spontaneously when no additional energy is required for double-twist rotations at large ρ. The latter may be achieved by permitting the magnitude of the moment to be soft. As shown in Figs. 12(c) and 13, skyrmions under these conditions have the lowest energy density, when the moment decreases with increasing distance from the centre.

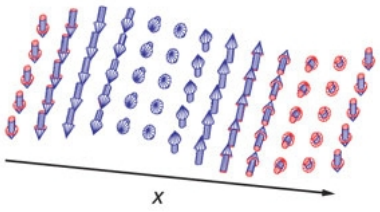

(a)One dimensional modulated structure propagating along a direction x with constant modulus of magnetic moments.

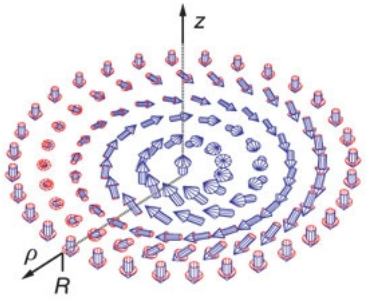

(b)Circular cross-section through a skyrmionic excitation with fixed modulus. The modulation has propagation axes in all directions ρ from the centre of a cylindrical tube.

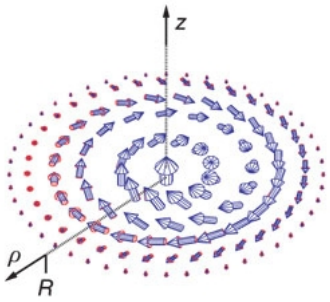

(c)A circular skyrmion cell. The magnetization has maximum modulus m at the skyrmion axis, $\rho = 0$, and equals zero at the cell boundary R.

FIG. 12 Three chiral modulated structures for noncentrosymmetric ferromagnets like MnSi. Figure from Roszler *et al.* (2006).

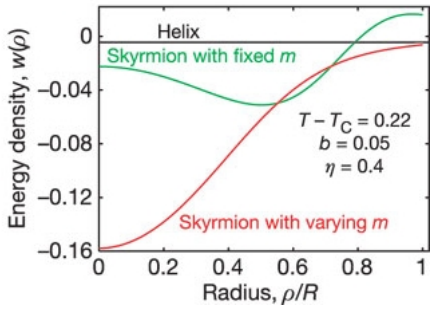

FIG. 13 Comparison for the local energy density per unit volume for the helical modulation in Fig. 12(a) and skyrmions with fixed and varying magnetic moment m (Figs. 12(b) and 12(c)), along a radial direction ρ. Figure from Roszler *et al.* (2006).

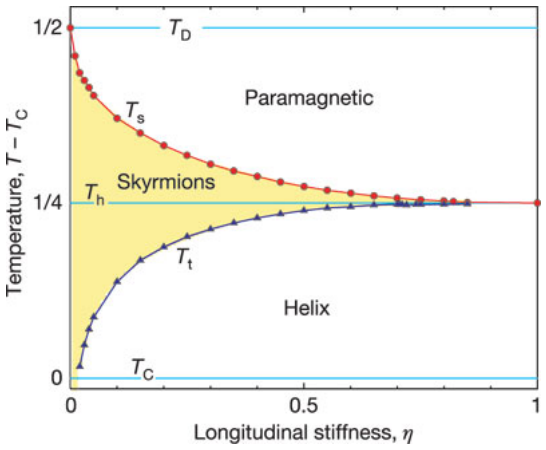

FIG. 14 Phase diagram of a chiral ferromagnet in terms of temperature versus longitudinal stiffness parameter (T,η). The diagram is based on the stability of the cylindrical skyrmions shown in Fig. 12(c). Above the ferromagnetic Curie temperature T_c two characteristic temperatures, equation (3.3), rule the phase diagram: T_D for the instability against double twisting and T_h for the formation of the helical phase. The skyrmion phase is stable between the line $T_s(\eta)$ for the continuous transition into the paramagnetic phase and the line $T_t(\eta)$ for the first-order transition into the helix. The helical phase exists as a metastable phase between T_h and $T_t(\eta)$. Figure from Roszler *et al.* (2006).

The results of a comprehensive numerical analysis of the free energy are summarized in Fig. 14 (see Eq. (3.1)). This establishes that stable cylindrical skyrmions form spontaneously in a finite temperature interval $T_t < T < T_s$ of the phase diagram. The magnetic structure of the skyrmions is characterized by a magnetization vector $\boldsymbol{m} = (m, \theta, \psi)$ that rotates outward from the axis in all directions, while the modulus $m(\rho)$ shrinks and decreases towards the boundary of the tube at radius R (Fig. 12(c)). It turns out that the amplitude of the local magnetization $m(\rho)$ vanishes continuously when approaching T_s from below. Thus, the skyrmion nucleation and the formation of the skyrmion texture coincide. The increase of the magnetization with decreasing temperature drives the transition from the skyrmion phase to the uniform helix phase at a lower temperature T_t. The transition into a one-dimensionally modulated state by transforming the structure in Fig. 12(b) or 12(c) into the helix 12(a) cannot be performed by a smooth deformation of the skyrmions, because these two textures have different topologies. For this reason (see Section I), a first-order transition is generally expected at a temperature T_t. In the phase diagram, the transition line T_t has been determined from the approximate condition that the average energy of the circular skyrmion cell is equal to that of the helix. The skyrmion phase vanishes as $T_s \to T_t$ in the limit $\eta \to 1$.

In a chiral magnet, the formation of an extended skyrmion condensate is now subject to: (1) weak residual magnetic anisotropies and dipolar interactions in the crystalline environment, and (2) the magnetization in the regime joining the skyrmion tubes. Under the most favourable conditions, the skyrmion condensate may form a regular lattice in analogy to the vortex lattice of type-II superconductors.

To illustrate the stability of a skyrmion condensate for this case, Roszler *et al.* (2006) have plotted the full solution for an extended state in an isotropic system in two dimensions, shown in Fig. 15. This applies also to three-dimensional systems, when the solutions are artificially constrained to remain homogeneous in the third spatial direction (perpendicular to the plane shown in Fig. 15). The structure of this solution shows in particular that the core region of the skyrmions is unaffected, while the magnetization between the skyrmions mediating their interactions does not even need to be strictly zero for the skyrmion lattice to become the ground state.

The spontaneous formation of skyrmions applies to all symmetry classes without inversion centre, because the modulus of the magnetization m and the polar angle θ– which control the energetic stability of the skyrmions, respectively are identical for all relevant symmetry classes (Bogdanov, 1995). In contrast, the behaviour of the azimuthal angle ψ affects only the manner of rotation of the magnetic moments in the radial direction. General considerations of the stability of localized textures for chiral magnets suggest that droplet-like skyrmions are not stable in three dimensions (Bogdanov, 1995). Therefore, it is probable that the two-dimensionally localized skyrmion tubes discussed so far will form extended ground-state condensates in three-dimensional systems.

However, in a three-dimensional environment bending and terminating skyrmion tubes imposes a cost in energy that determines the nature of the condensate. One therefore expects that the skyrmion condensate in isotropic three-dimensional materials may have a liquid-like or amorphous appearance, driven by the frustration between preferred orientations and their elastic interactions in the condensed structure.

The elementary mechanism for a ferromagnet (illustrated in Fig. 12) applies to any chiral system with a

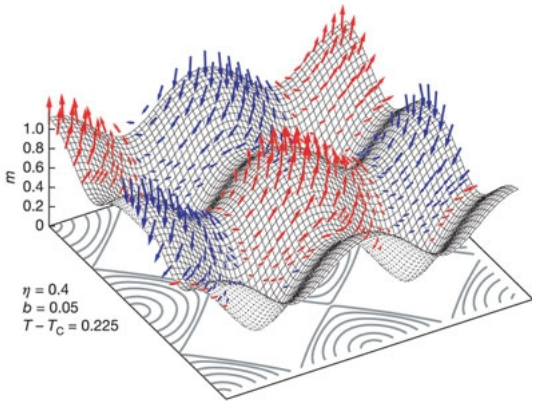

(a)Overview, showing the modulus m and the corresponding magnetization vectors.

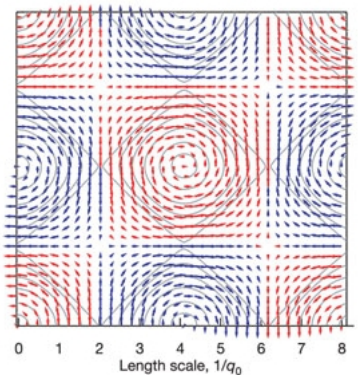

(b)Projection of the magnetization vectors into the base plane.

FIG. 15 Structure of a two-dimensional skyrmion lattice, derived as a minimum energy solution for Eq. (3.1) with Dzyaloshinskii–Moriya interactions. Red/blue signals label magnetization direction with positive/negative components. Contour lines stand for constant modulus, $m \equiv$ constant, in the skyrmion cores. The result applies to thin magnetic films with broken inversion symmetry make from isotropic or cubic metallic materials. A three-dimensional analogue of this dense texture composed of amorphous arrangement of cylindrical skyrmion strings is consistent with recent experiments in MnSi (see Section III.A). Figure from Roszler *et al.* (2006).

tendency to form twisted structures. In particular, this model also applies to antiferromagnetic crystals with chiral symmetry by replacing the magnetization with a staggered antiferromagnetic vector order parameter. Owing to the broken inversion symmetry at the surfaces of magnetic materials (Bogdanov and Roszler, 2001), thin films and interfaces are the largest class of condensed-matter systems in which skyrmion condensates may form spontaneously.

The results of Roszler *et al.* (2006) for $\eta < 1$ establish the possible existence of blue phases in chiral ferromagnets. Whereas the blue phases in chiral liquid crystals are stabilized by topological defects in the form of disclination lines, which do not exist in magnetic systems, skyrmion textures in chiral magnets emerge instead as a condensate of strictly localized skyrmions with lines or sheets of vanishing magnetic order between them (Fig. 15).

Fluctuations and the competition between different frustrated couplings imply the possibility of internal transitions between various textures with liquid, glassy or lattice-like organization of skyrmions.

2. Possible Evidence of Skyrmion Ground States in MnSi

We have seen that one expects the spontaneous formation of a skyrmion ground state in a temperature interval prior to helical order in all materials with soft magnetisation amplitude and weak chiral interactions. Bulk compounds which develop long-wavelength helical order of the kind considered here are, for instance, MnSi, where the modulation wavelength is $\lambda_{MnSi} \approx 180$ Å. In this material the helical modulation is driven by Dzyaloshinsky-Moriya chiral interactions that originate in the lack of inversion symmetry in their cubic B20 crystal structure (see Section III.A.1). Being transition metal compounds, the magnetic order is due to itinerant electrons. Polarised neutron scattering data exist for MnSi (Semadeni *et al.*, 1999) that establish a reduced longitudinal stiffness ($\eta_{\rm MnSi} = 0.4$). Thus *MnSi meets all the requirements for the formation of spontaneous skyrmion ground states.*

The helical order in MnSi, may be seen most easily in small-angle neutron scattering (SANS) experiments, where sharp magnetic satellites were observed. In a small temperature interval above the onset of helical order, SANS data for MnSi show neutron scattering intensity located on the surface of a sphere in reciprocal space as an additional feature.

The radius of this sphere corresponds to the same modulation length as the helical order. The sphere of scattering intensity has therefore traditionally been interpreted as fluctuating helical order. The scattering intensity on the surface of the sphere is perfectly consistent with randomly oriented cylindrical skyrmion tubes.

To identify the meaning of the ring of scattering intensity, here is a rough estimate of the temperature interval $\Delta T = T_D - T_c$, for which the skyrmion ground state is expected in MnSi. The lattice constant of MnSi is $a_{MnSi} = 4.55$ Å. There are four formula units per unit cell, so that the number-density is $N/V = n = 4.246{\cdot}10^{28}$ m^{-3}. The effective moment determined from the Curie-Weiss temperature dependence of the susceptibility is $p_{\rm eff} = 2.2\mu_B$ (Yasuoka *et al.*, 1978) and the susceptibility $\chi = C_{\rm CW}/(T - T_c)$ where $C_{\rm CW} = n\mu_0\mu_B^2(p_{\rm eff}^2)/(3k_B) = 0.534$ K. The upper limit of the skyrmion transition temperature is $T_h = T_c + (1/2)(D/(2A))(D/a)$ as given in Eq. (3.2) in Section III.B.1. These parameters have to be taken from experiment (Grigoriev *et al.*, 2005). The parameter a is given by the initial susceptibility and may be estimated from the Curie-Weiss susceptibility: $a = 1/(2C_{\rm CW}) = 0.936$ K^{-1}. The modulus of the helical propagation vector is $q_0 = (D/(2A)) =$

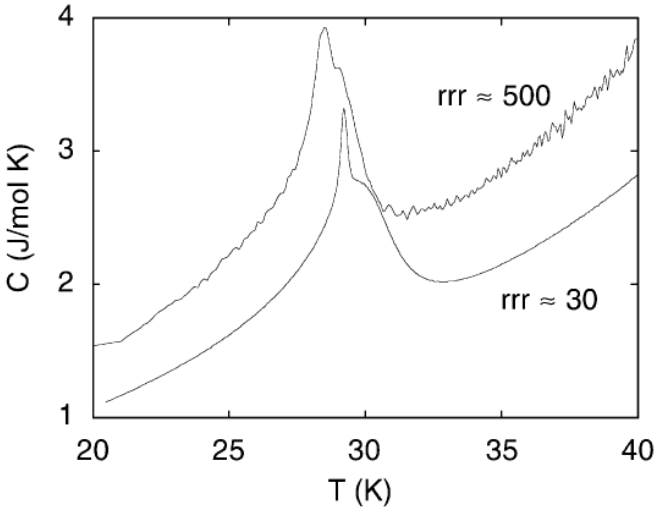

FIG. 16 Specific heat of two samples of MnSi of different purity at ambient pressure near T_c. The low-purity sample exhibits a smaller absolute value of C, even at low T. Figure from Pfleiderer (2001b).

0.039 Å^{-1}. Temperature is used as unit of energy-density. The exchange stiffness A may then be estimated from $A \simeq (a^2_{\rm MnSi})T_c = 50 \cdot 10^{-3}$ eV Å^2 = 587 K Å^2. The strength of the DM-coupling D may be estimated from q_0 as $D = 1.9 \cdot 10^{-3}$ eV Å= 22 K Å. These parameters finally result in $T_h = T_c + (1/2)q_0(D/a) = T_c + q_0 D C_{\rm CW} = (29.5 + 0.46)$ K. The ordering temperature of the skyrmion phase (according to Eq. (3.3) in Sec. III.B.1) is obtained by doubling the difference between T_c and T_h so that $\Delta T = T_D - T_c = 0.9$ K. This value of ΔT gives an order-of-magnitude estimate for the temperature interval of the stable skyrmion phase in MnSi as shown in the phase diagram of Fig. 14.

Fig. 16 shows the specific heat of the paramagnetic to helical transition in MnSi. Notice the presence of a broad shoulder in a temperature interval of order ~ 1 K above this transition. Detailed SANS studies of the ring of intensity as function of temperature suggest that the ring extends over the same temperature interval where the shoulder in the specific heat is seen. Interestingly, the temperature interval corresponds fairly well with that predicted for the skyrmion phase. In combination, the broad shoulder in the specific heat clearly signals the presence of quasi-static order already above T_h that may be either related to randomly oriented helical domains or an amorphous texture of skyrmions. An important additional aspect that has been emphasized by Pfleiderer (2001b) is that the shape of the specific heat anomaly in very high purity samples is quite different, but it still supports the possible existence of a precursor phase. However, the shoulder is observed for samples with largely varying *residual resistivity ratio* (rrr). The residual resistivity ratio is a measure of sample purity, with higher values signifying higher purity. It is possible that the dependence on extreme sample purity signals that the stabilisation of the quasistatic order sensitively depends on residual defects in the material.

The spontaneous formation of skyrmion ground states allows to explain many of the mysterious properties of MnSi at high pressure and low temperatures. As we saw in Section III.A, the metallic state of MnSi changes under pressure from the behaviour of a weakly spin-polarized Fermi liquid to an anomalous behaviour. The low temperature resistivity in MnSi changes abruptly from a T^2-Fermi liquid temperature dependence to a $T^{3/2}$ dependence above a pressure $p_c = 14.6$ kbar. Above p_c the resistivity is unchanged up to at least $3p_c$, suggesting the formation of a stable phase over a remarkably large pressure range. Three aspects appear to be inconsistent with the present day understanding of metallic magnetism: First, as pointed out in Sec. III.A, a $T^{3/2}$ resistivity is normally observed in spin glasses and amorphous ferromagnets, where it is explained by a diffusive motion of the charge carriers. See also the application of these ideas by Smith (2005) which tries to explain the $T^{3/2}$ resistivity as result of an inhomogeneous magnetic state in MnSi. Pfleiderer (2004) suggested a possible explanation by the temperature-dependence of the excitations in magnetic domain walls. This idea cannot apply for the resistivity in MnSi because one would then expect a $T^{3/2}$ resistivity also in the helically ordered state, which is equivalent to a succession of domain walls. Therefore the explanation of the anomalous $T^{3/2}$ resistivity by a very inhomogeneous magnetic state in MnSi under pressure is suggested through the comparison with the resistivity in spin-glasses. For the high-purity MnSi single-crystals investigated, however, the behaviour of a moderately enhanced Fermi liquid is expected by all accounts. It was therefore emphasized that the diffusive charge carrier motion would have to be intrinsic. Second, the $T^{3/2}$ resistivity is extremely stable as function of pressure, where it has been seen up to at least 45 kbar $\approx 3p_c$. This suggests the formation of an extended new phase in contrast to a cross-over phenomenon normally observed at quantum phase transitions. Third, the $T^{3/2}$ resistivity is extremely stable as function of magnetic field, where experiment shows that it collapses abruptly only above a certain critical field related to a so-called itinerant-electron metamagnetic transition (Thessieu, 1997). At the highest pressures the $T^{3/2}$ resistivity extends at least up to 1 T (Doiron-Leyraud *et al.*, 2003) which substantially exceeds the field needed to collapse helical order $B_c \approx 0.6$ T. We note that B_c studied by various magnetic probes is insensitive to pressure.

As a possible resolution to these contradictions Roszler *et al.* (2006) suggest that the Fermi liquid to non-Fermi liquid transition in MnSi may signal a transition between helical order and an amorphous skyrmion ground state. A spontaneous amorphous skyrmion ground state provides a simple intrinsic mechanism that explains why the transport properties of an amorphous ferromagnet are seen even in a high purity material in the absence of disorder or frustration. The leading order effect of pressure

in this scenario would be to generate a slight mode softening that reduces the stability of helical order, but not to collapse the magnetic moment on local scales completely as normally assumed at quantum phase transitions. Because the skyrmions form as a genuine, stable ground state, it would finally not be difficult to explain, a priori, the extent of the $T^{3/2}$ resistivity behaviour in the temperature-pressure phase-diagram. Also, it has been shown that the core of cylindrical skyrmion tubes is extremely stable against external fields (Bogdanov and Hubert, 1994). Thus, if the $T^{3/2}$ resistivity is due to an amorphous skyrmion texture, it is expected that the behaviour survives to much higher fields. The signature of such an amorphous skyrmion ground state in neutron scattering would be intensity on the surface of a small sphere in reciprocal space, similar to that seen at ambient pressure above T_h.

Neutron scattering studies of the magnetism as function of pressure indeed show that large ordered moments survive deep into the phase where the $T^{3/2}$ resistivity is observed (see end of Section III.A). The ordered moments are organised such that they lead to scattering intensity on the surface of a sphere in reciprocal space. There is, however, a very important difference with the intensity on a sphere seen at ambient pressure near T_h. The ambient pressure intensity is isotropic, while broad maxima are observed for $\langle 110 \rangle$ at high pressure. The $\langle 110 \rangle$ direction is unusual for this cubic magnet. This is so, because (i) the leading magnetocrystalline anisotropy favours easy magnetic axes only in $\langle 111 \rangle$ or $\langle 100 \rangle$ directions. And, (ii), in itinerant d-electron magnets as MnSi with very weak anisotropy, it is very unlikely that higher-order anisotropy contributions do play any role. In fact, the easy axis of the helical order in MnSi is $\langle 111 \rangle$. Thus, if there are randomly oriented helical order at high pressure in MnSi, it would be very difficult to explain the broad maxima along $\langle 110 \rangle$. In contrast, for a condensate of skyrmion tubes the odd maxima for $\langle 110 \rangle$ are easily explained, if one assumes that the easy magnetic axis of MnSi, $\langle 111 \rangle$, does not change as function of pressure, while the magnetism changes from a helical modulation along $\langle 111 \rangle$ to an amorphous texture with cylindrical skyrmion tubes having their axes preferentially along $\langle 111 \rangle$. For cylindrical skyrmion tubes that are stratified along $\langle 111 \rangle$, neutron scattering intensity in reciprocal space is expected on great circles perpendicular to $\langle 111 \rangle$ directions. As all $\langle 111 \rangle$ directions produce intensities along such great circles, these will intersect and produce maxima of intensity in the $\langle 110 \rangle$ directions. The available experimental data are consistent with this possibility.

However, in contrast to the remarkable extent of the $T^{3/2}$ resistivity under pressure and magnetic field, the sphere of scattering intensity under pressure is seen only in a fairly small portion of the phase diagram. A possible explanation discussed by Doiron-Leyraud *et al.* (2003) is that the textures are dynamically destabilized and become "invisible" in the neutron scattering experiment. Such a slowly "wandering" form of magnetic order could persist on a time scale that it still much slower than the time scale relevant to the electrical resistivity. A liquid instead of a frozen skyrmion phase in this pressure range provides a natural explanation for the difference in the transport measurements and the visible static magnetic order in neutron scattering. Such a liquid skyrmion phase would not be unusual and may be analoguous to liquid vortex phases in superconductors.

IV. DISCUSSION AND CONCLUSIONS

A. Summary of Review

In the introductory Section we have seen the basic features of Landau's theory of phase transitions, followed by modern treatments of both classical and quantum phenomena. In Section II, the essential concepts of a Fermi liquid were discussed, as well as possible ways in which this standard model of metals could go wrong. A fascinating example of Fermi liquid to non-Fermi liquid transition was presented in Section III, for the case of the itinerant-electron ferromagnet MnSi. Both experimental facts and theoretical predictions were discussed, with an emphasis on the peculiar temperature dependence of its resistivity.

B. Conclusion and Perspectives

The $T^{3/2}$ power law of the resistivity in MnSi measured in the seminal paper of Pfleiderer *et al.* (2001) constitutes a breakdown of the Fermi-liquid (or nearly ferromagnetic Fermi-liquid) model, long assumed to be valid for the normal state of itinerant-electron ferromagnets. Moreover, $T^{3/2}$ variations of the resistivity have also been observed in other itinerant-electron ferromagnets, notably $ZrZn_2$ and Ni_3Al. This suggests that the $T^{3/2}$ power law may have a general origin for this class of systems and might not be just a consequence of some peculiarity of MnSi.

The spontaneous formation of skyrmion ground states presented in Section III.B.1 allows one to explain many of the properties of MnSi at high pressures and low temperatures. A $T^{3/2}$ resistivity is normal in inhomogeneous systems like spin glasses and amorphous ferromagnets, where it is explained by a diffusive motion of the charge carriers. By comparison with the spin glasses, a very inhomogeneous magnetic state in MnSi (under pressure) was proposed. In this case however, the diffusive charge carrier motion would have to be *intrinsic*. A spontaneous amorphous skyrmion ground state provides this intrinsic mechanism. It also explains the persistence of this power law in very pure samples and high external magnetic fields.

Recent theories on the partial magnetic order in MnSi by Tewari *et al.* (2006) and Binz *et al.* (2006) also suggest inhomogeneous twisted states, but *without identify-*

ing the mechanism of stable skyrmions in such textures, as Roszler *et al.* (2006) have done.

Evidence for an amorphous texture of cylindrical skyrmion tubes in MnSi was seen in neutron scattering experiments, but only in a very small portion of its phase diagram, in a reduced range of pressures. A liquid skyrmion state in the rest of the phase diagram *could* be a possible explanation. However, this problem is still open, and further investigation will require the use of novel experimental techniques (such as Lorentz force microscopy and 3D polarisation analysis of neutron scattering) as well new theoretical developments.

Acknowledgments

I would like to thank my advisor Maxim Mostovoy for bringing this fascinating field to my attention and also for giving a *tip-top* course in Condensed Matter Theory!

References

Andres, K., J. E. Graebner, and H. R. Ott, 1975, Physical Review Letters **35**(26), 1779.
Baym, G., and C. Pethick, 1991, *Landau Fermi Liquid Theory* (Wiley, New York).
Belitz, D., and T. R. Kirkpatrick, 2007, Nature Physics **3**(1), 15.
Belitz, D., T. R. Kirkpatrick, and T. Vojta, 1997, Phys. Rev. B **55**(15), 9452.
Belitz, D., T. R. Kirkpatrick, and T. Vojta, 2005, Reviews of Modern Physics **77**, 579.
Binz, B., A. Vishwanath, and V. Aji, 2006, Phys. Rev. Lett. **96**, 207202.
Bogdanov, A., 1995, JETP Lett. **62**, 247.
Bogdanov, A., and A. Hubert, 1994, J. Magn. Magn. Mater. **138**, 255.
Bogdanov, A. N., and U. K. Roszler, 2001, Phys. Rev. Lett. **87**, 037203.
Doiron-Leyraud, N., I. R. Walker, L. Taillefer, M. J. Steiner, S. R. Julian, and G. G. Lonzarich, 2003, Nature **425**(6958), 595.
Dorfman, J. R., T. R. Kirkpatrick, and J. V. Sengers, 1994, Annual Review of Physical Chemistry **45**(1), 213.
Fischer, K. H., 1979, Z. Phys. B **34**, 45.
Ford, P., and J. A. Mydosh, 1976, Phys. Rev. B **14**, 2057.
Goto, T., Y. Shindo, H. Takahashi, and S. Ogawa, 1997, Phys. Rev. B **56**, 14019.
Grigoriev, S. V., S. V. Maleyev, A. I. Okorokov, Y. O. Chetverikov, R. Georgii, P. Boni, D. Lamago, H. Eckerlebe, and K. Pranzas, 2005, Physical Review B **72**(13), 134420.
Hertz, J. A., 1976, Physical Review B **14**(3), 1165.
Huxley, A., I. Sheikin, and D. Braithwaite, 2000, Physica B **284-288**, 1277.
Landau, L. D., 1956, Zh. Eksp. Teor. Fiz. **30**, 1058.
Landau, L. D., 1965, in *Collected Papers of L. D. Landau*, edited by D. T. Haar (Pergamon, Oxford).
Law, B. M., and J. C. Nieuwoudt, 1989, Phys. Rev. A **40**(7), 3880.
Mahan, G. D., 1990, *Many-Particle Physics* (Springer), 2nd edition.
Millis, A. J., 1993, Phys. Rev. B **48**, 7183.
Nagel, S. R., 1992, Rev. Mod. Phys. **64**(1), 321.
Pfleiderer, C., 2001a, Nature **412**, 660.
Pfleiderer, C., 2001b, Journal of Magnetism and Magnetic Materials **226**, 23.
Pfleiderer, C., 2004, Nature **427**, 227.
Pfleiderer, C., S. R. Julian, and G. G. Lonzarich, 2001, Nature **414**(6862), 427.
Pines, D., and P. Nozieres, 1990, *The Theory of Quantum Liquids*, volume I (Addison-Wesley, New York).
Rivier, N., and A. E. Mensah, 1977, Physica B **91**, 85.
Roszler, U. K., A. N. Bogdanov, and C. Pfleiderer, 2006, Nature **442**(7104), 797, ISSN 0028-0836.
Sachdev, S., 1999, *Quantum Phase Transitions* (Cambridge University Press, Cambridge).
Semadeni, F., P. Boni, Y. Endoh, B. Roessli, and G. Shirane, 1999, Physica B **268**, 248.
Skyrme, T. H., 1961, Proc. R. Soc. Lond. Ser. A **260**, 127.
Smith, M. F., 2005, Journal of Physics: Condensed Matter **17**(50), 8049.
Stoner, E. C., 1938, Proc. R. Soc. Lond. A **165**, 372.
Tewari, S., D. Belitz, and T. R. Kirkpatrick, 2006, Phys. Rev. Lett. **96**, 047207.
Thessieu, C., 1997, J. Phys. Condens. Matter **9**, 6677.
Uemura, Y. J., T. Goko, I. M. Gat-Malureanu, J. P. Carlo, P. L. Russo, A. T. Savici, A. Aczel, G. J. MacDougall, J. A. Rodriguez, G. M. Luke, S. R. Dunsiger, A. McCollam, *et al.*, 2007, Nature Physics **3**(1), 29.
Varma, C. M., 1985, Physical Review Letters **55**(24), 2723.
Varma, C. M., Z. Nussinov, and W. van Saarloos, 2002, Physics Reports **361**(5-6), 267.
Vojta, T., D. Belitz, R. Narayanan, and T. R. Kirkpatrick, 1996, Europhysics Letters (EPL) **36**(3), 191.
van der Waals, J. D., 1873, *On the continuity of the gas and liquid state*, Ph.D. thesis, University of Leiden.
Weiss, P., 1907, J. Phys. Theor. Appl. **6**, 667.
Widom, B., 1965, The Journal of Chemical Physics **43**(11), 3892.
Wilson, K. G., and Kogut, 1974, J. Phys. Rep. **12**, 75.
Yasuoka, H., V. Jaccarino, R. C. Sherwood, and J. H. Wernick, 1978, J. Phys. Soc. Jpn **44**, 842.